Diplomarbeit

Reduced density matrix approach to the laser-assisted electron transport in molecular wires

vorgelegt von:
Sven Welack

TECHNISCHE UNIVERSITÄT
CHEMNITZ

Fakultät für Naturwissenschaften
Professur Theorie ungeordneter Systeme

Chemnitz, November 30, 2005

Referent: Professor Dr. Michael Schreiber
Koreferent: Professor Dr. Heinrich Solbrig
Betreuer: Priv.-Doz. Dr. Ulrich Kleinekathöfer

Abstract

The electron transport through a molecular wire under the influence of an external laser field is studied using a reduced density matrix formalism. The full system is partitioned into the relevant part, i.e. the wire, electron reservoirs and a phonon bath. An earlier second-order perturbation theory approach of Meier and Tannor for bosonic environments which employs a numerical decomposition of the spectral density is used to describe the coupling to the phonon bath and is extended to deal with the electron transfer between the reservoirs and the molecular wire. Furthermore, from the resulting time-nonlocal (TNL) scheme a time-local (TL) approach can be determined. Both are employed to propagate the reduced density operator in time for an arbitrary time-dependent system Hamiltonian which incorporates the laser field non-perturbatively. Within the TL formulation, one can extract a current operator for the open quantum system. This enables a more general formulation of the problem which is necessary to employ an optimal control algorithm for open quantum systems in order to compute optimal control fields for time-distributed target states, e.g. current patterns. Thus, we take a fundamental step towards optimal control in molecular electronics. Numerical examples of the population dynamics, laser controlled current, TNL vs. TL and optimal control fields are presented to demonstrate the diverse applicability of the derived formalism.

TABLE OF CONTENTS

Chapter

Chapter 1

INTRODUCTION

Nowadays semiconductor industry is already working towards 65 nanometer and smaller scales [INT] in order to fabricate commercially used integrated circuits. After 40 years, it is questionable whether Moore's law, i.e. a doubling of the number of transistors in a given space every 12 months [Moo65] (later corrected to every 24 month), will still describe the grade of miniaturization over the next decades. By reaching the physical limits of atomic structure engineers face tough challenges like quantum tunneling and excessive heat generation.

Thus, a completely new type of technology is required and different major approaches have been pursued over the years. For instance, the broad field of spintronics utilizes an additional physical quantity of the electron, namely the spin, to store and manipulate information within the conventional semiconductor environments [WAB+01, ŽFS04]. Another possibility is to replace the "top-down" engineering of todays semiconductor heterostructures by a "bottom-up" approach which leads one directly to the field of molecular electronics [NR03, GDDN04]. It was the idea of Aviram and Ratner published in their milestone paper [AR74] to construct molecular rectifiers in addition to common p-n structures. A complex molecule consisting of tetracyanoquinodimethane (TCNQ) and tetrathiofulvalene (TTF), which, if connected to each other by methylene (CH_2), act as electron acceptor and donor, respectively, should be placed between two metal leads and work as an rectifier due to its asymmetric electrical properties and the internal tunneling barrier.

Since then, the general goal of the field has been to realize electrical circuits by assembling and arranging single molecules in the desired way. First steps were to measure experimentally and to describe theoretically the electrical conductance properties of a metal-molecule-metal junction. Early experiments utilized the scanning-tunneling microscope (STM) technique to measure the distance-current characteristics of a single C_{60} molecule at room temperature [JGSC95]. Also, xylyl-dithiol (XYL) molecules on a gold film were bounded to nanometer size Au-clusters realizing a gold-dithiol-gold junction for which the voltage-current characteristics was measured with an STM tip and estimates for the resistance of a single XYL molecule were obtained [DGO+95]. In a similar way, an atomic force microscope was used

for measurements of the conductivity of octanedithol molecules within an isolating monolayer on a gold surface bound to gold nanoparticles [CPZ+01]. The experiment proved that a chemical bond between the molecule and the metallic contacts is required to approach intrinsic molecular properties. Later STM experiments employing a self-assembled monolayer of xylyl-dithiol and phenyl-dithiol molecules on a metallic surface showed a good agreement between the measured and theoretically calculated I-V curves of a junction realized by a small number of molecules [TDH+98]. The disadvantage of the STM approach is a lack of long-term stability of the junction. The current-voltage characteristic depends beside the intrinsic electronic structure of the molecule also on the properties of the vacuum barrier separating the tip and the sample. Furthermore, the tip establishes only a weak contact situation.

The second major experimental branch employs mechanically controllable break junctions (MCB) [RZM+97, SNU+02, ROW+02, KBP+99], where a piezo element controls the distance between two electrodes with a large reduction factor between its elongation and separation of the contacts. The break junctions can be fabricated using electron-beam lithography to structure a gold film [ROW+02] or by just using a notched gold wire [RZM+97]. Breaking the junction mechanically engenders sharp gold contacts which then form a stable and adjustable tunneling junction. Molecules in a solution can enter the region between the contacts and realize the desired metal-molecule-metal junction. With this method it was possible to measure the current-voltage characteristic of benzene-1,4-dithiol molecules at room temperature [RZM+97] and of an ensemble of bisthiolterthiophene molecules [KBP+99]. By comparing symmetric and asymmetric molecules with thiol end groups, it was possible to reproduce spatial (and therefore intrinsic) properties of molecules from a measured I-V characteristic [ROW+02]. Also, an inorganic hydrogen molecule was used to realize single channel conductance at low temperatures [SNU+02] which unambiguously proves the feasibility of single molecule junctions.

On the down-side, the specific details of the geometry of the break junction are unknown and it is generally hard to verify unambiguously whether only one molecule contributes to the current within the junction. Beside the discussed examples, there exist a broad variety of promising candidates for molecular wire system. Important criteria are self-assemblance and chemically controllable fabrication as well as electronic properties which qualify the system to act as a current rectifier, switch or gate. Thus, the prospect of using DNA strings as molecular wires is intriguing since they have the potential for self-assemblance [YPF+03], but whether they provide the necessary electrical properties is still subject to scientific discussion [WWR05]. Also carbon nanotubes [Iij91], especially single-wall nanotubes, have been considered to act as molecular wires and transport measurements showed excellent electrical properties [TDD+97]. For instance, coherent electron transport between two leads

with a distance of 140 nm was realized by utilizing almost one-dimensional conduction modes. Furthermore, the proposal to use single-walled nanotubes as chemical sensors [KFZ+00], e.g. measurements showed a dependence between resistivity and exposure to different gas molecules, leads to applications beyond current switches and rectifiers. However, on the contrary to DNA, carbon nanotubes have poor manufacturing properties which have to be improved if one wants to complement todays semiconductor technology.

For a sufficient description of the metal-molecule-metal junction, theorists face a variety of theoretical challenges. First, one has to deal with the constraint of the macroscopic electron reservoirs which are defined on a completely different scale as the molecule. Therefore, a description of a quantum open system is required. Similar to experiments where little is known about the molecule-metal bridge, one formally has to deal with the electron transfer between the wire and the lead in a different way than with the intrinsic charge transport in the molecule. Also, a realistic model of the intrinsic electron transfer mechanism requires a simulation of the molecular orbitals as well as an understanding of the involvement of the vibrational effects due to an additional phonon-bath coupling. Furthermore, the problem also necessitates a nonequilibrium kinetic approach, since the coupling to the leads, bias voltages and especially external laser fields can cause dynamical effects which are not approachable by a simple description of the equilibrium state of the system.

While calculations of the conductance spectrum [TDH+98, MKR94, Nit01, GGS02] employing different methods indicate a good agreement with the experimental data, dynamical aspects are harder to treat theoretically. Several communities have started to approach the problem with methods related to their field of study and were able to cover the problem to a certain extent. But a transport formalism which describes these kinds of system without making inconvenient assumptions or approximations is still demanded. A powerful tool in mesoscopic physics is the Landauer-Büttiker scattering formalism [Lan57, BILP85, Bue86, Dat95] and condensed matter physicists could calculate with it especially regimes governed by a strong wire-lead coupling, e.g. through thiol groups. Especially in the case of steady state currents, the results for the conductance spectrum of these kinds of strongly coupled molecules were successful [TDH+98], despite the rough approximation of the quantum open system. The infinite gold contacts were approximated by only a few gold atoms and additional self-energy functions. The approach employed an extended Hückel method [Hof63] to compute the density of states of the LUMO and HOMO band of the molecule. Within the Landauer-Büttiker formalism, coherent transport is seen as transmission [IL99] attenuated by elastic scattering processes. Its original phenomenological derivation could later be proven by linear respone theory [BS89], which adds another physical restriction namely small bias voltages. In its

original form, the formalism is unable to address dynamical time-dependent effects within the system and despite recent extensions to oscillating fields [DA92, WJM93], the non-equilibrium kinetic aspects of the problem are still hard to cover.

Density functional theory (DFT) as an atomistic level description has been very successful to describe the electronic properties of molecules as well as the band structure of bulk structures. In combination with non-equilibrium Greens functions (NEGF) it was possible to address time-dependent transport through molecular systems [KSA+]. NEGF calculations are formally embedded within the vast area of transport theory [GDDN04], since it can be shown that they are conform with the Boltzmann formalism in the case of band-like transport and also reduce to a Landauer-Büttiker description in the absence of dephasing processes, i.e. inelastic scattering. Despite the advantage, that the energetic levels within the wire are modeled in a realistic way, the initial Greensfunctions are constructed from single particle DFT calculations and many-body effects are only approximated. In reference [EWK04] it is pointed out that approximations made to account for the particle-exchange are not valid in a weak wire-lead coupling regime. Another challenge within the formalism is to take environmental effects, e.g. vibrational coupling to a photon bath, into account as well as to find a description that extends it beyond semi-finite electron reservoirs. A more recent approach based on DFT is the time-dependent current-DFT [UV02], but it still fails to respect the important system conditions implied by the metallic leads.

On the contrary to DFT based studies, empirical tight-binding descriptions model general physical situations and are not apriori related to specific examples like a certain molecule. Thus, it is not possible to make computations that can be directly compared to a measurement. But by employing a tunneling model Hamiltonian with the corresponding tight-binding parameters one can identify major physical phenomena which then might be observable in an attenuated form in molecular systems. For instance, the effect of current induced light emission [GN] could be demonstrated by using NEGF calculations. Early works using a master equation approach to study electrical currents in quantum dots [BS93, BBS97] showed its potential in respect to describe the quantum open system, the coupling to an external field and time-dependent transport. Approaches based on Floquet-states proved quite applicable to the case of periodic laser fields, since the periodic time-dependence of the field is already included by defining rotating eigenstates and expressions are derived within the theoretical framework of their static counterparts. This led to impressive results for the electron transport in periodically driven systems within scattering approaches [KARM02] and methods based on a master equation description [LCKH03, LKHN03, LKMH04, KLH05, LKHN02, CKH04, CLKH03, LLY+05, CLSY]. For instance, conductance resonance [KARM02], current rectifiers [LKHN03, LKHN02], electron pumps [BS93, BBS97], and coherent current control

[LKMH04, LCKH03, RSK$^+$] were demonstrated. Furthermore, results for highly dynamical effects like current fluctuations [KCS$^+$04, CKH04, CLKH03] were obtained. The advantage of the master equation description is that the vibrational coupling is usually addressed in a similar way as the coupling in the electron reservoirs. One only has to apply different statistics, namely Bose statistics and Fermi statistics respectively, and different operators to each process [LKMH04]. In general, coupling to a much larger dissipative environment engenders quantum decoherence in the system since it reduces the entanglement of the system states. The quantum properties of the system are no longer measurable and the system evolves into its "classical analog". In terms of transport theory, this corresponds to a transition from a purely coherent transport regime, where transport is realized by transport channels, to an incoherent regime dominated by a sequential nearest neighbor hopping process.

Only very little is known about effects caused by arbitrary time-dependent fields which cannot be treated by methods based on Floquet states and only a few approaches were published in this field [ON05, KSA$^+$, YX05], recently. The broad field of dissipative quantum mechanics includes sophisticated methods to deal with arbitrary time-dependent Hamiltonians within a dissipative environment. Here, the influences of monochromatic laser fields [Dak94, GKS95, GPM96, CDM97, GH98] or short laser pulses [SM98, MT99] on molecular systems are also widely studied. Thus, we adopt a method developed by Meier and Tannor [MT99] which is based on the time-nonlocal (TNL) Nakajima-Zwanzig identity [Nak58, Zwa61] and modify it to account for the electron transfer between an electron reservoir and a molecular wire which is described by an empirical tight-binding Hamiltonian. Furthermore, we will directly apply their method to realize the vibrational coupling of the wire to a phonon bath. It was shown [XY02, Kle04] that the approach of Meier and Tannor can be extended to derive similar equations in a time-local (TL) scheme, something we utilize to rewrite the presented formalism into a TL picture. Similar to other master equation approaches, the wire lead coupling is treated in second-order perturbation theory while the laser field is included non-perturbatively.

In order to describe relaxation on ultra-short time scales correctly, one needs to incorporate memory effects [MT99, XY02, Kle04]. To be able to apply the Markovian approximation, i.e. the neglect of memory effects onto the relaxation, one has to assume that the correlation times of the environment are much larger than the time scales of the internal dynamics in the wire. The approach of Meier and Tannor avoids the Markov approximation which allows the formalism to deal with the influence of the electrical field on the current in the wire on a femto-second scale.

Once having a formalism at hand to compute time-dependent currents on ultra-short time scales, one can approach the next challenging step, namely to derive an applicable method to optimize the external laser fields which are supposed to control the current dynamically. Previous numerical works on time-dependent currents in

molecular wires applied time-periodic fields with special amplitude to frequency ratios to cause the previous mentioned effects [LCKH03, LKHN03, LKMH04, KLH05, LKHN02, CKH04, CLKH03]. Since typical molecular energies are in the region of eV, the prospective of an active control of chemical reactions with ultra-short laser pulses in chemistry spurred major theoretical and experimental efforts. In the feedback control algorithms utilized in experiments, a computer analyzes the data from a previous measurement by employing an evolutionary algorithm to optimize the parameters of the control field which is then applied in the following measurement procedure [JR92]. Thus, a self-learning loop is defined.

First theoretical investigations of the control problem resulted in the pump-dump molecular control scheme of Tannor, Kosloff and Rice [TKR86] and the optimal control theory (OCT) of Rabitz et al. [SR90]. In general, OCT optimizes a control functional under defined constraints and due to this generality, it was successfully applied to a variety of different systems in physics and chemistry [Yan93, SVR99, OZR99]. Furthermore, recent publications could successfully extend OCT to the field of dissipative quantum mechanics [MM01, MKM02, Oht03, XYO$^+$04].

Here, we adopt an optimal control mechanism for dissipative systems based on a reduced density matrix approach [MM01, MKM02] and modify it to derive optimal laser pulses controlling electrical currents in molecular wires. Many situations in molecular dynamics have the defined control goal to excite the system into a certain state for a short moment in time in order to cause a chemical reaction or physical process. But the optimization of the electrical current towards a defined value at a single moment in time would not be of much interest in molecular electronics, where a certain current pattern as a function of time, e.g. a Gaussian current spike, is required to process information. Recent formal extensions to control states that are distributed in time [KM05b, KM05a] suggest a way to treat the time-dependent current phenomena and to obtain optimized current patterns as a function of time. Thus, we will combine both approaches and propose the first step leading to optimal control of molecular electronics by deriving an optimal control formalism for the laser driven wire.

This thesis is organized as follows. In chapter 2, we give a short introduction to the density operator formalism and derive an equation of motion (EOM) by applying the Nakajima-Zwanzig identity and second-order perturbation theory to the reduced density operator coupled to a dissipative environment. In chapter 3, we deal with the description of a more specific model for the system, e.g. the molecular wire, and its environment consisting of the electron reservoirs and a phonon bath. In chapter 4, the derived EOM is transformed into a set of equations that can be numerically propagated in time by utilizing a decomposition of the spectral density. Starting from the EOM of the reduced density operator, a current equation is derived in TNL and TL form, before we present the corresponding numerical results in chapter 6.

The current equation in TL form enables one to derive a current operator. This gives one the generality required to apply optimal control theory to the problem as presented in chapter 7. The thesis is concluded with a final summary and outlook.

Chapter 2

DENSITY OPERATOR FORMALISM AND NAKAJIMA-ZWANZIG IDENTITY

2.1 The statistical operator

A quantum mechanical state $|\Psi(t)\rangle$ does not refer to a physical situation in the same way as the classical concepts of coordinates and momenta of mass points or electromagnetic fields since it represents a set of probability distributions [Bal98]. For each state $|\Psi(t)\rangle$ a unique statistical operator can be postulated as

$$\rho(t) = |\Psi(t)\rangle\langle\Psi(t)|. \tag{2.1}$$

The corresponding space of state $|\Psi(t)\rangle$ is spanned by the denumerable and orthogonal basis $|\Psi(t)\rangle = \sum_n a_n(t)|\phi_n\rangle$. The conventional normalization of $|\Psi(t)\rangle$ directly implies a normalization of the statistical operator $\mathrm{tr}\{\rho(t)\} = 1$. The density operator formalism is an elegant description of quantum mechanics since it addresses the statistical aspects involving statistical ensembles of states as well as the subtle concepts of measurement and entanglement of states [EPR35] in a convenient way. The expectation value of the observable $\langle Q\rangle$ is given by

$$\langle Q\rangle = \mathrm{tr}(\rho Q), \tag{2.2}$$

where Q is a self-adjoint operator defined in the Hilbert space of $\rho(t)$. This leads directly to a second restriction on $\rho(t)$, namely that

$$\rho(t) = \rho^\dagger(t) \tag{2.3}$$

in order to ensure that observables of the system (the quantum mechanical counterparts of the classical concepts) have real values. The property of the statistical to be nonnegative is proven by

$$\langle\phi_n|\rho(t)|\phi_n\rangle = |a_n(t)|^2 \geq 0. \tag{2.4}$$

Applying its normalization, one can derive for the statistical operator defined in Eq. (2.1) the following equality

$$\rho^2(t) = |\Psi(t)\rangle\langle\Psi(t)||\Psi(t)\rangle\langle\Psi(t)| = \rho(t). \tag{2.5}$$

Within the framework of the density operator formalism, property (2.5) is usually employed to differentiate between pure states and statistical ensembles for which the relation $\mathrm{tr}\{\rho^2(t)\} \leq \mathrm{tr}\{\rho(t)\} = 1$ applies. The statistical operator for statistical ensembles or statistical mixtures is defined by

$$\rho(t) = \sum_n W_n |\Psi_n(t)\rangle\langle\Psi_n(t)|. \tag{2.6}$$

Here, we have a situation where the system manifests itself in a number of different states $|\Psi_n(t)\rangle$ with corresponding probability W_n. The normalization of $\rho(t)$ implies the restrictions $1 \geq W_n \geq 0$ and $\sum_n W_n = 1$. The physical situation described by a statistical ensemble is a preparation of a system several times in a similar way resulting in a probability distribution over a mixture of states. Furthermore, the diagonal elements of $\rho(t)$ are the probability to find the system in a certain state, while the off-diagonal elements are the coherences containing the phase information of the system. Thus, the off-diagonal elements distinguish between a quantum mechanical situation, where one observes effects due to different phases of states, and a classical situation described within the framework of quantum mechanics, without any phase relation between independently prepared states. The concept of decoherence describes the transition between both. Concerning semantics, we will also refer to the statistical operator as density operator since it describes a distribution of probabilities or density matrix once a set of basis vectors for the system is defined.

2.2 Time evolution of statistical mixtures

The time evolution from the initial time t_0 to time t of the quantum mechanical state $|\Psi(t)\rangle$ for a time-dependent Hamiltonian $H(t)$ is given by the solution of the Schrödinger equation

$$|\Psi(t)\rangle = \vec{T} e^{-\frac{i}{\hbar}\int_{t_0}^{t} \mathrm{d}\tau H(\tau)} |\Psi(t_0)\rangle. \tag{2.7}$$

$\vec{T}$ is the time ordering operator in positive time direction. For a statistical mixture described by the density operator, Eq. (2.7) becomes

$$\rho(t) = \vec{T} e^{-\frac{i}{\hbar}\int_{t_0}^{t} \mathrm{d}\tau H(\tau)} \rho(t_0) e^{\frac{i}{\hbar}\int_{t_0}^{t} \mathrm{d}\tau H(\tau)} = U(t, t_0)\rho(t) \tag{2.8}$$

and the time evolution operator $U(t, t_0)$ is defined as

$$U(t, t_0) = \vec{T} e^{-\frac{i}{\hbar}\int_{t_0}^{t} \mathrm{d}\tau \mathcal{L}(\tau)}. \tag{2.9}$$

Writing Eq. (2.8) in its differential form results in the Liouville-von Neumann equation

$$\frac{\partial \rho(t)}{\partial t} = -\frac{i}{\hbar}[H(t), \rho(t)] = -\frac{i}{\hbar}\mathcal{L}(t)\rho(t). \tag{2.10}$$

The Liouville operator $\mathcal{L}(t)$ is defined as a commutator with the Hamilton operator. From now on, we set $\hbar = 1$ to simplify the notation.

2.3 Nakajima-Zwanzig identity and reduced density matrix approach

In general, the EOM of the complete density operator $\rho(t)$ including the wire and the leads is given by the Liouville-von Neumann equation. In a situation, where a small quantum mechanical system is coupled to a much larger environment describable in terms of statistics, the information of interest is limited only to the inner (or relevant) system part and contained in the reduced density operator $\rho_S(t)$. In this section, we shortly present the derivation of the Nakajima-Zwanzig operator identity [Nak58, Zwa61, Zwa64] and utilize it to couple a dissipative environment to the relevant system.

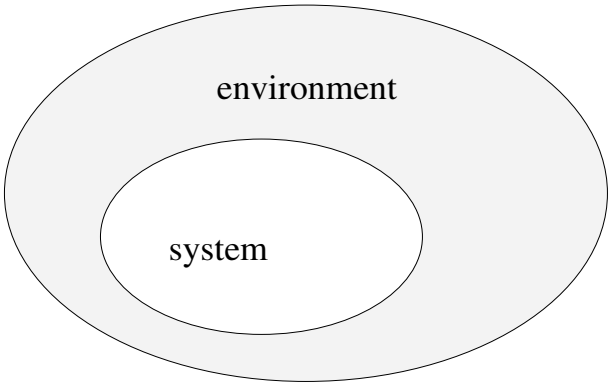

Figure 2.1: The relevant system and its environment.

One can define a projection operator P, with $P^2 = P$, which acts on an arbitrary operator A defined in the Hilbert space of the complete system

$$PA = \mathrm{B}\,\mathrm{tr}_B\{A\}. \tag{2.11}$$

B is an operator defined in the environmental part only, with $\mathrm{tr}_B(B) = 1$. Applying the projection operator to the density operator of the full system leads to

$$P\rho(t) = \rho_B\,\mathrm{tr}_B\{\rho(t)\} = \rho_B \otimes \rho_S(t). \tag{2.12}$$

Thus, the EOM for the complete system can be written as

$$\dot{\rho}(t) = -i\mathcal{L}(t)\rho(t) = P\dot{\rho}(t) + (1-P)\dot{\rho}(t) = -i\mathcal{L}(t)P\rho(t) - i\mathcal{L}Q\rho(t) \tag{2.13}$$

which can be interpreted as the evolution of the projected part $P\rho(t)$ plus the evolution of its orthogonal complement $Q\rho = (1-P)\rho$. Furthermore, applying the projection operator to the Liouville-von Neumann equation and to its orthogonal complement leads to

$$P\dot{\rho}(t) = -iP\mathcal{L}(t)P\rho(t) - iP\mathcal{L}(t)Q\rho(t) \tag{2.14}$$

and

$$Q\dot{\rho}(t) = -iQ\mathcal{L}(t)P\rho(t) - iQ\mathcal{L}(t)Q\rho(t), \tag{2.15}$$

respectively. Integrating the differential equation of the orthogonal complement part (2.15) and applying it to Eq. (2.14) results in the Nakajima-Zwanzig operator identity

$$\begin{aligned} P\dot{\rho} &= -iP\mathcal{L}(t)P\rho(t) - iP\mathcal{L}(t)\vec{T}e^{-i\int_{t_0}^{t}\mathrm{d}\tau(1-P)\mathcal{L}(\tau)}(1-P)\rho(t_0) \\ &\quad + P\mathcal{L}(t)\int_{t_0}^{t}\mathrm{d}t'\,\vec{T}e^{-i\int_{t'}^{t}\mathrm{d}\tau(1-P)\mathcal{L}(\tau)}(1-P)\mathcal{L}(t')P\rho(t') \end{aligned} \tag{2.16}$$

which is valid for arbitrary time-dependent Hamiltonians. Since all the operators are chronologically ordered in time, the literature refers to this time-nonlocal (TNL) approach often as chronological time ordering prescription (COP)[MOR78, RBN97, Yan98] or time convolution approach [BKP99]. We will refer to this approach as TNL to point out that the dissipation term includes the memory of the system contained in the density operator $\rho(t')$.

One can further simplify this expression by tracing out the environmental part of the density matrix employing the property of the projection operator $\mathrm{tr}_B\{P\dot{\rho}(t)\} = \dot{\rho}_S(t)$ in order to derive

$$\dot{\rho}_S(t) = -i\mathcal{L}_S(t)\rho_S(t) - i\mathrm{tr}_B\{\mathcal{L}_{SB}\rho_B\} + \int_{t_0}^{t}\mathrm{d}t'K(t,t')\rho_S(t') + \mathrm{In}(t) \tag{2.17}$$

where the Kernel $K(t,t')$ reads

$$K(t,t') = -\mathrm{tr}_B\{\mathcal{L}_{SB}(t)\vec{T}e^{-i\int_{t'}^{t}\mathrm{d}\tau(1-P)\mathcal{L}(\tau)}(1-P)(\mathcal{L}_B(t') + \mathcal{L}_{SB}(t'))\rho_B\} \tag{2.18}$$

and the initial value term is given by

$$\mathrm{In}(t) = -i\mathrm{tr}_B\{\mathcal{L}_S(t)\vec{T}e^{-i\int_{t_0}^{t}\mathrm{d}\tau(1-P)\mathcal{L}(\tau)}(1-P)\rho(t_0)\}. \tag{2.19}$$

Here, we have assumed that the Liouville operator of the system depicted in Fig. 2.1 can be formally separated into terms describing the evolution within the relevant system $\mathcal{L}_S$, the environment $\mathcal{L}_B$ and the interaction $\mathcal{L}_{SB}$ between both.

Up to this point, all transformations are exact in the sense that we did not employ any algebraic approximations. But in order to derive an applicable method to solve Eq. (2.17), we utilize second order perturbation theory [Haa73, Blu96, MT99] by assuming that $(1-P)\mathcal{L}_{SB} \approx 0$ or $\mathcal{L}_{SB} \approx P\mathcal{L}_{SB}$, what implies for the Kernel $K(t,t')$ that

$$e^{-i(1-P)\mathcal{L}t} = e^{-i(1-P)(\mathcal{L}_S+\mathcal{L}_B+\mathcal{L}_{SB})t} \approx e^{-i(1-P)(\mathcal{L}_S+\mathcal{L}_B)t}. \tag{2.20}$$

Therefore, we demand that the coupling between the environment and the relevant system is weak, or in other words, that the dissipation process is slower than the internal dynamics of the relevant system. The technical advantage of assumption (2.20) is that we will able to separate the relevant system parts from the environment terms in the Kernel $K(t,t')$. One could also realize a straightforward expansion of $e^{-i(1-P)\mathcal{L}_{SB}t}$, but this would lead to inapplicable summations in the dissipation term. Without presenting a proof, we can further simplify Eq. (2.17) by making use of the following algebraic exact relations:

$$\mathcal{L}_B\rho_B = 0, \tag{2.21}$$

$$P\mathcal{L}_{SB}\rho_B = 0, \tag{2.22}$$

$$e^{-i(1-P)\mathcal{L}t} = P + (1-P)e^{-i\mathcal{L}t}, \tag{2.23}$$

$$\mathrm{tr}_B\{\mathcal{L}_{SB}PC\} = 0 \tag{2.24}$$

for an arbitrary operator C. Finally, neglecting the initial value term (2.19) in the evolution of the reduced density matrix results in the Liouville equation with a dissipation term in a TNL regime

$$\dot{\rho}_S(t) = -i\mathcal{L}_S(t)\rho_S(t) - \mathrm{tr}_B\{\mathcal{L}_{SB}(t)\int_{t_0}^{t} \mathrm{d}t' U_{S+B}(t,t')\mathcal{L}_{SB}(t')\rho(t')\} \tag{2.25}$$

In the next chapter we will define a specific model for the relevant system and its environment and then employ Eq. (2.25) to realize the coupling. For the system, we will employ a tight-binding Hamiltonian which already includes the time-dependent external laser field. Thus, the environment of the wire consists of the electron reservoirs and a thermal phonon bath.

Chapter 3

DESCRIPTION OF THE WIRE AND ITS ENVIRONMENT

3.1 The molecular wire and the coupling to the electron reservoirs

The system of interest, depicted in Fig. 3.1, can be represented in a very general form by the time-dependent Hamiltonian

$$H(t) = H_S(t) + H_R + H_{SR} \tag{3.1}$$

which consists of the time-dependent part describing the relevant system $H_S(t)$, an Hamiltonian describing the electron reservoirs H_R, acting in the presented study as electronic leads, and a coupling term H_{SR} between the relevant system and the reservoirs. The orbital description of the wire consists of its electronic sites n which are coupled to each other by a hopping parameter Δ. In second quantization, this orbital tight-binding description of the molecular wire reads

$$H_S(t) = \sum_{nn'} H_{nn'}(t) c_n^\dagger c_{n'} \tag{3.2}$$

where c_n annihilates and $c_n^\dagger$ creates an electron at site n. The fermionic properties of the electrons are reflected in the anticommutator relations

$$[c_n^\dagger, c_{n'}]_+ = \delta_{n,n'} \tag{3.3}$$

and

$$[c_n, c_{n'}]_+ = [c_n^\dagger, c_{n'}^\dagger]_+ = 0. \tag{3.4}$$

In the present study the time-dependence of $H_S(t)$ is only due to the irradiation of the system by an external time-dependent electromagnetic field that manipulates the on-site energies E_n with a time-dependent on-site potential $U_n(t)$. By neglecting possible influences of the external field on the tight-binding hopping parameter Δ, the matrix elements $H_{nn'}(t)$ can be decomposed into

$$H_{nn'}(t) = -\Delta(\delta_{n+1,n'} + \delta_{n,n'+1}) + (E_n + U_n(t))\delta_{nn'}. \tag{3.5}$$

Since we do not include any spin effects, the wire Hamiltonian does not take correlation between electrons with opposite spin into account. Furthermore, the Coulomb repulsion of the electrons is also neglected. Both exchange mechanisms lead to important effects in certain regimes and more detailed future investigations will include them.

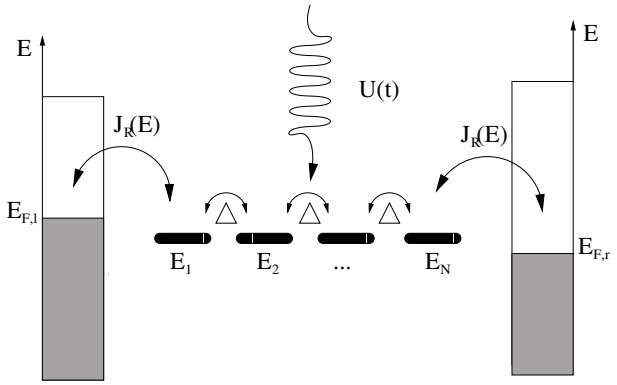

Figure 3.1: We study a multi-site system with the two outermost sites attached to electron reservoirs in thermal equilibrium with their respective Fermi energies $E_{F,l}$ and $E_{F,r}$. The coupling of the outermost sites to the corresponding lead is described by a spectral density function $J_R(\omega)$. The sites are connected to each other by a hopping element Δ. The on-site energies E_n for $(n = 1, ..N)$ of the wire can be manipulated with a time-dependent external electrial field $U(t)$.

The environment of the wire consists of two electronic leads that are modeled by two independent electron reservoirs in thermal equilibrium. For each lead, the Hamiltonian H_R in second quantization is given by

$$H_R = \sum_q \omega_q c_q^\dagger c_q \tag{3.6}$$

with $c_q^\dagger$ and c_q creating and annihilating an electron in the corresponding bath mode $|q\rangle$ with mode energy ω_q. Due to the assumed thermal equilibrium of the electron reservoirs, the occupation expectation values of the bath modes are determined by

$$\mathrm{tr}\{c_q^\dagger c_{q'} \rho\} = n_F(\omega_q - E_F)\delta_{qq'}, \tag{3.7}$$

where n_F is the Fermi function and E_F the Fermi energy. The left and the right electronic leads are coupled to the first site and to the last site of the wire, respectively. To keep the notation simple, we will only refer to the left lead in further derivations

but the formalism has to be applied to the right lead as well. The coupling of the left electronic lead with the first site of the wire reads in second quantization

$$H_{SR} = \sum_q (V_q c_1^\dagger c_q + V_q^* c_q^\dagger c_1) \tag{3.8}$$

with a system-lead coupling strength V_q for each bath mode q. In general, these coupling values are determined by the the electronic bands of the contacts that couple with the energy levels of the wire and by the occupation level of these bands with electrons given by the Fermi function and energy.

3.2 The coupling to a dissipative phonon bath

Besides the coupling to the electronic leads, the wire can also be subject to a thermal phonon-bath, as it is depicted in Fig. 3.2. Phonons are quantized vibrations of a rigid lattice which is in the presented study represented by the one dimensional wire. The Hamiltonian of the whole system reads

$$H(t) = H_S(t) + H_R + H_{SR} + H_{Ph} + H_{SPh}. \tag{3.9}$$

The free phonon bath Hamiltonian is given by

$$H_{Ph} = \sum_q \epsilon_q a_q^\dagger a_q \tag{3.10}$$

and $a_q^\dagger$, a_q create and annihilate a phonon in bath mode q with mode energy ϵ_q, respectively. Since phonons are bosonic particles, their creation and annihilation operators obey the corresponding commutator relations $[a_q, a_{q'}] = [a_q^\dagger, a_{q'}^\dagger] = 0$ and $[a_q, a_{q'}^\dagger] = \delta_{q,q'}$. If a system is in thermal equilibrium, the occupation distribution of the phonon bath can be obtained within the framework of Bose statistics as

$$\mathrm{tr}\{a_q^\dagger a_{q'} \rho\} = n_B(\epsilon_q)\delta_{qq'}, \tag{3.11}$$

where $n_B(\epsilon_q)$ is the Bose function. In general, the wire phonon-bath coupling Hamiltonian reads

$$H_{SPh} = \sum_n^N \mathrm{X}_{nn'} c_{n'}^\dagger c_n \sum_q \Upsilon_q (a_q + a_q^\dagger). \tag{3.12}$$

Here, the phonon position operator $a_q + a_q^\dagger$ interacts with either the electron number operator $c_n^\dagger c_n$ of site n, if $n = n'$, or the intersite hopping operator, if $n \neq n'$. Both are parameterized by the bath-wire coupling strength Υ_q. On the contrary to the wire-lead hopping Hamiltonian (3.8), Hamiltonian (3.12) does not describe a particle but an energy exchange. Thereby it determines the regime of electron transfer in the

wire [LKHN02, LKHN03]. We will also assume that each site n couples to exactly one of identical sets of bath modes, i.e.

$$X_{nn'} = \delta_{nn'}. \tag{3.13}$$

The algebraic structure of Hamiltonian (3.12) is also similar to coupling terms between a phonon bath and a system described by electronic excitations [KBH+03], despite the fact that the underlying physical processes are different.

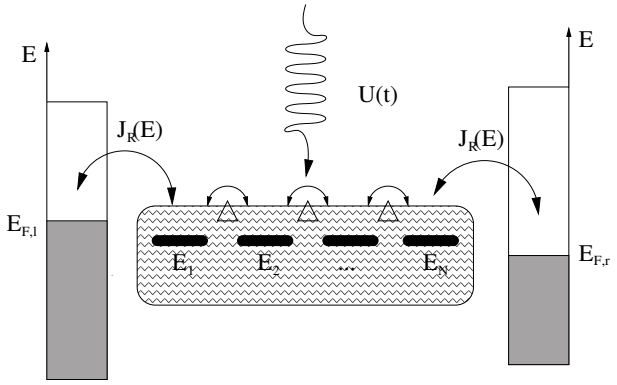

Figure 3.2: Same physical situation as in Fig. 3.1 but with an additional phonon bath applied to the wire.

3.3 The many-body Fock space

In order to realize a numerical investigation of the problem, one has to choose an appropriate basis for the Hilbert space of the relevant system which is described by its reduced density operator (2.25). We will use an orbital representation consisting of a geometric arrangement of wire sites and every single site can be in two distinct states. Either it is occupied by an electron $|1\rangle$ or unoccupied $|0\rangle$. Thus, the quantum mechanical state vector of the wire site n is formed by the superposition

$$|\chi_n\rangle = \alpha_n|0\rangle + \beta_n|1\rangle, \tag{3.14}$$

where α_n and β_n are the corresponding coefficients. A possible representation of the two state description is given by the vectors

$$|0\rangle = \begin{pmatrix} 1 \\ 0 \end{pmatrix}$$

$$|1\rangle = \begin{pmatrix} 0 \\ 1 \end{pmatrix} \tag{3.15}$$

which imply the following matrices for the annihilation and creation operators

$$c_n^\dagger = \begin{pmatrix} 0 & 0 \\ 1 & 0 \end{pmatrix}, \quad c_n = \begin{pmatrix} 0 & 1 \\ 0 & 0 \end{pmatrix}. \tag{3.16}$$

A total state vector $|\Psi\rangle_\zeta$ for the relevant system can be constructed from the set of site state vectors of the wire connected by the tensor product

$$|\Psi\rangle_\zeta = |\chi_1, \chi_2, ..., \chi_N\rangle_\zeta = (|\chi_1\rangle \otimes |\chi_2\rangle \otimes ... \otimes |\chi_N\rangle)_\zeta \tag{3.17}$$

All the employed operators, e.g. the reduced density matrix, the annihilation and creation operators, are defined in the many-body Fock space spanned by the set of state vectors (3.17) An effective way to construct their matrices is to consider them as superpositions of the form $|\Psi\rangle_\zeta\langle\Psi|_{\zeta'}$. For instance, in the case of a two site system $c_1 = |0,1\rangle\langle 1,1| + |0,0\rangle\langle 1,0|$. Since it is defined as a projector in Fock space, the reduced density matrix contains all possible local and global states of the wire. Due to its fermionic algebra which has its foundations in the proper choice of the on-site annihilation and creation operators (3.16), the Fock space is intrinsically symmetrized and includes the Pauli exclusion principle. Since the vectors (3.15) are normalized, the state vectors of the Fock space (3.17) are normalized as well. We will not have to find an algebraic representation for the electron reservoirs and the phonon bath because they are treated statistically in our model. The disadvantage of the Fock space is that it scales with 2^N, what makes it numerically inapplicable for larger and higher dimensional systems.

3.4 The dipole operator

The external field can cause a manifold of effects within the molecule and the environment, depending on its amplitude and frequency. For instance, it could heat the electron gas and cause mechanical expansions of the leads which would alter the lead-wire coupling strength. Due to formal reasons, we sometimes have to separate the Hamiltonian of the system into a tight-binding part H_{tb}, including the on-site energies and the sequential hopping, and a field part $H_\mu(t)$, which includes all the interactions with the electric field

$$H_S(t) = H_{tb} + H_\mu(t). \tag{3.18}$$

Because we want to define a simple model to study fundamental effects, we limit the interaction of the field with the system to a single dipole operator μ modulated by an arbitrarily time-dependent field strength $A(t)$:

$$H_\mu(t) = A(t)\mu. \tag{3.19}$$

In some calculations, we also employ the Liouville dipole operator given by

$$\mathcal{L}_\mu(t)\bullet = [H_\mu(t), \bullet] = A(t)[\mu, \bullet] = A(t)\mathcal{L}_\mu\bullet \tag{3.20}$$

Similar to recent studies [LIH02, LKHN03, LCKH03, LKMH04, LKHN02, KLH05, KCS+04] and in conformance with the empirical description of the molecular wire, we also pursue the idea of a dipole-like operator

$$\mu = e\sum_n x_n \tag{3.21}$$

where the scaled position of site n is defined as

$$x_n = \frac{(N+1-2n)}{2} c_n^\dagger c_n. \tag{3.22}$$

This simply corresponds to a situation of an asymmetric modulation of the on-site energies and neglects any intra-molecular dipole moments one would find in realistic molecules. Possible field enhancements caused by the presence of the metallic leads [JDHD98] which would attenuate the observability of effects which depend on a certain field strength are also neglected.

Chapter 4

TIME EVOLUTION OF THE REDUCED DENSITY MATRIX

The evolution of the reduced density operator is determined by three components: the intrinsic evolution determined by the wire Hamiltonian, the coupling to the electron reservoirs and the coupling to the phonon bath. By employing the Nakajima-Zwanzig identity and second-order perturbation theory (2.25), the three components of the full system can be decomposed into the following parts

$$\dot{\rho}_S(t) = -i\mathcal{L}_S(t)\rho_S(t) + D_{SR}(t,t_0) + D_{SPh}(t,t_0). \tag{4.1}$$

This chapter is dedicated to the derivation of EOM for the operators realizing the coupling to the electron reservoirs $D_{SR}(t,t_0)$ and to the thermal phonon bath $D_{SPh}(t,t_0)$. In general, these operators are given by the coupling term of Eq. (2.25) and therefore include the memory of the system.

4.1 The coupling to the electronic leads

4.1.1 Factorization of the system-reservoir coupling

The influence of the coupling to the electron reservoirs on the EOM of $\rho_S(t)$ can be extracted from Eq. (2.25) and reads

$$\dot{\rho}_S(t) = -i\mathcal{L}_S(t)\rho_S(t) - \mathrm{tr}_R\{\mathcal{L}_{SR}(t)\int_{t_0}^{t} \mathrm{d}t' U_{S+R}(t,t')\mathcal{L}_{SR}(t')\rho(t')\} \tag{4.2}$$

where we applied Eq. (3.8) as the transfer Hamiltonian between relevant system and environment. The annihilation and creation operators of the system and the environment are defined in different Hilbert spaces which makes it possible to rewrite the coupling Hamiltonian in Eq. (3.8) as

$$H_{SR} = \sum_x K_x \otimes \Phi_x \tag{4.3}$$

with $\Phi_1 = \sum_q V_q c_q$, $\Phi_2 = \sum_q V_q^* c_q^\dagger$ and $K_1 = c_1^\dagger$, $K_2 = c_1$. In order to evaluate Eq. (4.2) one has to take the following steps. After applying Eq. (4.3) to Eq. (4.2), the time-evolution operator U_{S+R} is separated into a system part and a reservoir part

$$U_{S+R}(t,t') = U_S(t,t')U_R(t,t') \tag{4.4}$$

with the evolution operator of the relevant system given by

$$U_S(t,t') = \vec{T} e^{-\frac{i}{\hbar}\int_{t'}^{t} \mathrm{d}\tau \mathcal{L}_S(\tau)}. \tag{4.5}$$

Furthermore, one can use the definition of the time-independent reservoir Liouville operator $\mathcal{L}_R$ to integrate the evolution operator of the reservoir

$$U_R(t,t')\bullet = \vec{T} e^{-\frac{i}{\hbar}\int_{t'}^{t} \mathrm{d}\tau \mathcal{L}_R}\bullet = e^{-iH_R(t-t')} \bullet e^{iH_R(t-t')}. \tag{4.6}$$

Thus, a non-Markovian quantum master equation in the Schrödinger picture can be obtained [MK00, LLY+05, Kle04]

$$\begin{aligned} \dot{\rho}_S(t) &= -i\mathcal{L}_S(t)\rho_S(t) - \int_{t_0}^{t} \mathrm{d}t' \,\mathrm{tr}_R\{[\sum_x K_x \otimes \Phi_x, \\ &\quad U_s(t,t')e^{-iH_R(t-t')}[\sum_{x'} K_{x'} \otimes \Phi_{x'}, \rho_S(t',t_0)]e^{iH_R(t-t')}]\}. \end{aligned} \tag{4.7}$$

A rearrangement of the summation over x and x' simplifies Eq. (4.7) to

$$\begin{aligned} \dot{\rho}_S(t) &= -i\mathcal{L}_S(t)\rho_S(t) \\ &\quad - \int_{t_0}^{t} dt' \sum_{xx'} \mathrm{tr}_R\{[K_x\Phi_x, U_S(t,t')e^{-iH_R(t-t')}[K_{x'}\Phi_{x'}, \rho_S(t',t_0)]e^{iH_R(t-t')}]\}. \end{aligned} \tag{4.8}$$

After writing out the two commutators in this dissipation term, one can summarize the trace over the reservoir degrees of freedom and all the reservoir operators into the following reservoir correlation functions

$$C_{xx'}(t) = C^*_{xx'}(-t) = \mathrm{tr}_R\{e^{iH_R t}\Phi_x e^{-iH_R t}\Phi_{x'}\rho_R\} \tag{4.9}$$

which contain all the intrinsic information about the reservoir. For the system of interest, these correlation functions decay in time thereby causing a memory loss in the dissipation term of Eq. (4.8). Due to the thermal equilibrium condition of the electronic leads, two of the four functions are zero,

$$C_{11} = C_{22} = 0. \tag{4.10}$$

This reduces the summation over x and x' to the pairs $(xx') = (12)$ and $(xx') = (21)$. By using the property of the reservoir correlation functions, i.e. $C_{xx'}(t) = C^*_{xx'}(-t)$,

and rearranging the terms of Eq. (4.8), we can write the master equation in terms of the correlation functions

$$\dot{\rho}_S(t) = -i\mathcal{L}_S(t)\rho_S(t) - \int_{t_0}^{t} dt' \sum_{xx'} [K_x,\, U_S(t,t')K_{x'}\rho_S(t')]C_{xx'}(t-t') \tag{4.11}$$

$$+[U_S(t,t')\rho_S(t')K_{x'},\, K_x]C^*_{x'x}(t-t'). \tag{4.12}$$

Furthermore, one can define the following auxiliary operators

$$\Lambda_{xx'}(t) = \int_{t_0}^{t} \mathrm{d}t' C_{xx'}(t-t')U_S(t,t')K_{x'}\rho_S(t') \tag{4.13}$$

$$\widehat{\Lambda}_{xx'}(t) = \int_{t_0}^{t} \mathrm{d}t' C^*_{x'x}(t-t')U_S(t,t')\rho_S(t')K_{x'} \tag{4.14}$$

to simplify Eq. (4.11). These auxiliary operators incorporate the memory of the system and weight the time-dependent electron transfer between the wire and the lead. Writing the quantum master equation (4.11) in terms of Eqs. (4.13, 4.14), we get the final expression

$$\dot{\rho}_S(t) = -i\mathcal{L}_S(t)\rho_S(t) - \sum_{xx'} [K_x,\, \Lambda_{xx'}(t) - \widehat{\Lambda}_{xx'}(t)] \tag{4.15}$$

for the master equation of the reduced density operator at time t. In the next subsection, we will deal with the derivation of EOM for the auxiliary operators (4.13, 4.14).

4.1.2 Spectral decomposition of the electron reservoir correlation functions

In analogy to methods recently developed for systems coupled to a bosonic bath [MT99, LLY+05, Kle04], we develop EOM for the auxiliary operators defined by Eqs. (4.13, 4.14) using a numerical decomposition of the spectral density $J(\omega)$ to decompose the reservoir correlation functions. Solving the trace in Eq. (4.9) and making use of Eq. (3.7), the nonvanishing bath correlation functions read

$$C_{12}(t) = \mathrm{tr}_R\{\sum_{qq'} V_q V^*_{q'} c_q e^{-i\omega t} c^\dagger_{q'}\rho_R\} = \sum_q |V_q|^2 n_F(-\omega_q + E_F)e^{-i\omega_q t} \tag{4.16}$$

$$C_{21}(t) = \mathrm{tr}_R\{\sum_{qq'} V^*_q V_{q'} c^\dagger_q e^{i\omega t} c_{q'}\rho_R\} = \sum_q |V_q|^2 n_F(\omega_q - E_F)e^{i\omega_q t}. \tag{4.17}$$

All the external properties of the fermionic lead are described by a single quantity, namely the spectral density $J(\omega)$ which can be generated by a superposition of weighted delta functions

$$J_R(\omega) = \sum_q \pi |V_q|^2 \delta(\omega - \omega_q). \tag{4.18}$$

Eq. (4.18) becomes a smooth function for a dense spectrum of the reservoir modes. Employing the properties of the δ function to transform the summation over q into an integral over ω, Eqs. (4.16, 4.17) can be written as

$$C_{21}(t) = \int_0^\infty \frac{\mathrm{d}\omega}{\pi} J_R(\omega)\, n_F(\omega - E_F) e^{i\omega t} \tag{4.19}$$

$$C_{12}(t) = \int_0^\infty \frac{\mathrm{d}\omega}{\pi} J_R(\omega)\, n_F(-\omega + E_F) e^{-i\omega t}. \tag{4.20}$$

To solve these integrals, we employ a method based on the same mathematical principles as the approach of Meier and Tannor [MT99] for bosonic systems (which is presented in the next section to account for the phonon bath).

On the contrary to the coupling to a phonon bath, we have to deal with two reservoir correlation functions since Hamiltonian (3.8) consists of two physically distinct processes, namely an electron enters the wire or an electron leaves the wire. Thus, the two algebraic distinct functions $C_{12}(t)$ and $C_{21}(t)$ account for these two processes. Furthermore, the single bath correlation function (for further detail please notice references [MT99, Kle04] and section 4.2) which describes the phonon bath has integral limits reaching from $-\infty$ to ∞ due to the algebraic form of the vibrational coupling Hamiltonian (3.12) consisting of only one distinct phonon bath operator, i.e. the position operator $a^\dagger + a$. In fact, if one would add the two reservoir correlation functions (4.19) (4.19) and assumes an asymmetric spectral density $J_{Ph}(\omega) = -J_{Ph}(-\omega)$, the sum would equal the single bath correlation function appearing in the phonon bath coupling term.

Here, the trick is to extend the lower limits in Eqs. (4.19, 4.20) to $-\infty$ by assuming that

$$J_R(\omega) \approx 0 \;\text{ for }\; \omega \leq 0, \tag{4.21}$$

since we need an improper form of the integrals to solve them by employing the theorem of residues later on. Thus, we derive our final integral equations for the reservoir correlation functions as

$$C_{21}(t) = \int_{-\infty}^\infty \frac{\mathrm{d}\omega}{\pi} J_R(\omega)\, n_F(\omega - E_F) e^{i\omega t} \tag{4.22}$$

$$C_{12}(t) = \int_{-\infty}^\infty \frac{\mathrm{d}\omega}{\pi} J_R(\omega)\, n_F(-\omega + E_F) e^{-i\omega t}. \tag{4.23}$$

A numerical decomposition that obeys condition (4.21) can be constructed by employing a single Lorentzian (instead of the two Lorentzian in the phonon bath case [MT99, Kle04])

$$J_R(\omega) = \sum_{k=1}^{m} \frac{p_k}{4\Omega_k} \frac{1}{(\omega - \Omega_k)^2 + \Gamma_k^2}, \tag{4.24}$$

with the real fitting parameters p_k, Ω_k and Γ_k which must be chosen with respect to condition (4.21),i.e. $\Omega_k > 0$ and $\Omega_k \ll \Gamma_k$. This decomposition is not restricted to a certain shape of the spectral density and can therefore be used to approximate complicated band structures. This enables one to avoid the assumption of the wide-band approximation [LIH02, LKHN03, LCKH03, LKMH04, LKHN02, KLH05, KCS+04] and to take influences of the band structure on the electron transfer between the wire and the lead fully into account. With the complex roots of the Fermi function and of function (4.24), the theorem of residues applied to Eqs. (4.22, 4.23) results in

$$C_{12}(t) = \sum_{k=1}^{m} \frac{p_k}{4\Omega_k\Gamma_k} n_F(-\Omega_k^- + E_F) e^{-i\Omega_k^- t} - \frac{2i}{\beta} \sum_{k}^{m'} J_R(\upsilon_k^*) e^{-i\upsilon_k^* t} \tag{4.25}$$

$$C_{21}(t) = \sum_{k=1}^{m} \frac{p_k}{4\Omega_k\Gamma_k} n_F(\Omega_k^+ - E_F) e^{i\Omega_k^+ t} - \frac{2i}{\beta} \sum_{k}^{m'} J_R(\upsilon_k) e^{i\upsilon_k t} \tag{4.26}$$

with the abbreviations $\Omega_k^+ = \Omega_k + i\Gamma_k$ and $\Omega_k^- = \Omega_k - i\Gamma_k$ and $\upsilon_k = i\frac{2\pi k+\pi}{\beta} + E_F$. The υ_k terms have the same mathematical origin as the Matsubara frequencies (4.44) but are related to the Fermi function and we technically refer to them as Fermi function residue (FFR) values. Eqs. (4.25, 4.26) determine the coefficients necessary to finally write the correlation functions as a superpostion of weighted exponential functions:

$$C_{12}(t) = \sum_{k=1}^{m+m'} a_{12}^k e^{\gamma_{12}^k t}, \tag{4.27}$$

$$C_{21}(t) = \sum_{k=1}^{m+m'} a_{21}^k e^{\gamma_{21}^k t}. \tag{4.28}$$

Rigorously, the sum over the FFR values would be infinite but it can be truncated at a finite value depending on the temperature of the system T and the spectral width of $J_R(\omega)$.

4.1.3 Propagation of the auxiliary density matrices and the reduced density operator

Since Eqs. (4.27 4.28) give us a representation of the reservoir correlation functions where the time argument is limited to the exponent, a set of differential equations for the auxiliary density operators can be derived by evaluating the total time derivative of Eqs. (4.13, 4.14), viz

$$\frac{\partial}{\partial t}\Lambda_{xx'}^k(t) = a_{xx'}^k K_{x'}\rho_S(t) - i[H_S(t), \Lambda_{xx'}^k(t)] + \gamma_{xx'}^k \Lambda_{xx'}^k(t), \tag{4.29}$$

$$\frac{\partial}{\partial t}\widehat{\Lambda}_{xx'}^k(t) = \left(a_{x'x}^k\right)^* \rho_S(t) K_{x'} - i[H_S(t), \widehat{\Lambda}_{xx'}^k(t)] + \left(\gamma_{x'x}^k\right)^* \widehat{\Lambda}_{xx'}^k(t), \tag{4.30}$$

with $\Lambda_{xx'}(t) = \sum_{k=1}^{m+m'} \Lambda^k_{xx'}(t)$ and $\widehat{\Lambda}_{xx'}(t) = \sum_{k=1}^{m+m'} \widehat{\Lambda}^k_{xx'}(t)$. These equations can be solved numerically using a simple Runge-Kutta method without the need of diagonalizing the Hamiltonian. Together with Eq. (4.15), one now has a complete set of differential equations describing the population dynamics in the wire coupled to an electric lead in second-order perturbation theory for an arbitrary time-dependent wire Hamiltonian. Regarding the right lead, one just needs to add a second dissipation term to the master equation (4.15) with differently defined K_x operators, i.e. acting on the last wire site N, and a second corresponding set of differential equations for the auxiliary operators.

4.2 The vibrational coupling

4.2.1 Factorization of the system-bath coupling

In order to couple the phonon bath to our system, we also utilize the techniques applied in the last section to describe the electron transfer. Furthermore, since the method we modified in the last section has its origin in the field of dissipative quantum mechanics where it was developed to account for bosonic environments [MT99, Kle04], we can apply it here without making any major modifications. The only difference is that in the case of the molecular wire, the phonon bath couples to different electronic sites instead to a multi-level harmonic oscillator, a fact we took already care of by the defintion of the phonon-wire coupling Hamiltonian (3.12). Following the notation of the last section, we can write the H_{PhS} as

$$H_{PhS} = \sum_n^N K_n \otimes \Phi \tag{4.31}$$

by defining $\Phi = \sum_q \Upsilon_q (a_q + a_q^\dagger)$ and $K_n = c_n^\dagger c_n$. Here we also used approximation (3.13). Employing again EOM (2.25) to account for the additional term $D_{SPh}(t)$ in Eq. (4.1) caused by the influence of the phonon bath, i.e. Eq. (4.31), leads to the dissipation term

$$D_{SPh}(t) = -\int_{t_0}^{t} \mathrm{d}t' \sum_n^N \mathrm{tr}_{Ph}\{[K_n\Phi, U_S(t,t')e^{-iH_{Ph}(t-t')}[K_n\Phi, \rho(t',t_0)]e^{iH_{ph}(t-t')}]\}. \tag{4.32}$$

One can summarize the trace over the bath degrees of freedom into a single phonon-bath correlation function

$$C(t) = C^*(-t) = \mathrm{tr}_{Ph}\{e^{iH_{Ph}t}\Phi e^{-iH_{Ph}t}\Phi\rho_{Ph}\}, \tag{4.33}$$

which contains the intrinsic information of the phonon bath. After solving all the commutator relations in Eq. (4.32) and defining the auxiliary operators

$$\Theta_n(t) = \int_{t_0}^{t} \mathrm{d}t' C(t-t')\, U_S(t,t') K_n \rho_S(t',t_0) \tag{4.34}$$

$$\widehat{\Theta}_n(t) = \int_{t_0}^{t} \mathrm{d}t' C^*(t-t')\, U_S(t,t')\rho_S(t',t_0)K_n \tag{4.35}$$

which contain the memory of the system, the dissipation term can be expressed as

$$D_{SPh}(t) = -\sum_{n}^{N}[K_n,\, \Theta_n(t) - \widehat{\Theta}_n(t)]. \tag{4.36}$$

4.2.2 Spectral decomposition of the phonon bath

The bath correlation function can be computed by inserting the definitions of the operators into Eq. (4.33), tracing out the expectation values by applying the thermal equilibrium condition of the phonon bath (3.11) and the commutator relations of bosonic creation and annihilation operators. This results in

$$C(t) = \mathrm{tr}_{Ph}\left\{\sum_{qq'} \Upsilon_q \Upsilon_{q'}(e^{-i\epsilon t}a_q + a_q^\dagger e^{i\epsilon t})(a_q + a_q^\dagger)\rho_{Ph}\right\} \tag{4.37}$$

$$= \sum_q |\Upsilon_q|^2 \left(1 + n_B\left(\epsilon_q\right)\right) e^{-i\epsilon_q t} + n_B(\epsilon_q)e^{i\epsilon_q t}. \tag{4.38}$$

The spectral density can be represented by a sum over the phonon bath modes

$$J_{Ph}(\epsilon) = \sum_q \frac{\pi}{2}|\Upsilon_q|^2\delta(\epsilon - \epsilon_q). \tag{4.39}$$

The interaction of each bath mode with the wire is given by its coupling strength Υ_q. Using the properties of the δ-function to extend the limit of the integral to $-\infty$ while assuming

$$J_{Ph}(\epsilon) = -J_{Ph}(-\epsilon), \tag{4.40}$$

one can transform the sum into the integral

$$C(t) = \int_{-\infty}^{\infty} \frac{\mathrm{d}\epsilon}{\pi}\, J_{Ph}(\epsilon) n_B(\epsilon) e^{i\epsilon t}. \tag{4.41}$$

This is just a mathematical trick to extend the limit of the integral to $-\infty$. The numerical decomposition of Meier and Tannor[MT99]

$$J_{Ph}(\epsilon) = \sum_{k=1}^{m} \frac{p_k}{4\Omega_k}\left(\frac{1}{(\epsilon - \Omega_k)^2 + \Gamma_k^2} - \frac{1}{(\epsilon + \Omega_k)^2 + \Gamma_k^2}\right) \tag{4.42}$$

respects the antisymmetric restriction made for negative frequencies and is not restricted to a special form of spectral density. The spectrum of the phonon bath $J_{Ph}(\epsilon)$ can be approximated by an Ohmic spectral density of the form $J(\omega) =$

$\eta\omega\exp(-\omega/\omega_c)$ with exponential cutoff [Kle04], which can numerically be represented by a superposition of Lorentzians as given by Eq. (4.42).

The time-integration in Eq. (4.41) is solved analytically by using the kernels residues, what leads to

$$\begin{aligned} C(t) &= \sum_k^m \frac{p_k}{4\Omega_k\Gamma_k}\Big((1+n_B(\Omega_k-i\Gamma_k))\,e^{-i(\Omega_k-i\Gamma_k)t} \\ &\quad +n_B(\Omega_k+i\Gamma_k)e^{i(\Omega_k+i\Gamma_k)t}\Big) + \frac{2i}{\beta}\sum_k^{m'} J_{Ph}(i\kappa_k)e^{-\kappa_k t}. \end{aligned} \tag{4.43}$$

κ_k are the Matsubara frequencies of the Bose function n_B given by

$$\kappa_k = \frac{2\pi k}{\beta}. \tag{4.44}$$

This equation determines the coefficients to write the bath-correlation function as a superpostion of weighted exponential functions

$$C(t) = \sum_k^{m+m'} b_k e^{\alpha_k t}. \tag{4.45}$$

Eq. (4.45) determines the coefficients of the set of differential equations for the auxiliary operators (4.34) (4.35)

$$\frac{\partial}{\partial t}\Theta_n^k(t) = b_k K_n \rho_S(t) - i[H_S(t), \Theta_n^k(t)] + \alpha_k \Theta_n^k(t) \tag{4.46}$$

$$\frac{\partial}{\partial t}\widehat{\Theta}_n^k(t) = b_k^* \rho_S(t) K_n - i[H_S(t), \widehat{\Theta}_n^k(t)] + \alpha_k^* \widehat{\Theta}_n^k(t). \tag{4.47}$$

These equations are propagated in time along with Eq (4.15), (4.29), (4.30) and (4.32). For the auxiliary terms in Eq. (4.32), one has to sum up the set of differential equations over the coefficients of the bath-correlation function at every time step of the propagation

$$\Theta_n(t) = \sum_k^{m+m'} \Theta_n^k(t), \tag{4.48}$$

$$\widehat{\Theta}_n(t) = \sum_k^{m+m'} \widehat{\Theta}_n^k(t). \tag{4.49}$$

4.3 Alternative time-local approach

Since we started with the Nakajima-Zwanzig identity to derive the EOM for the population dynamics the final expressions are in a time-nonlocal (TNL) form. In this section, we shortly present their time-local (TL) counterparts without giving an extended comparison of both approaches [Kle04]. In the literature, the time-local (TL) approach is also known as time-convolutioness formalism [BKP99], partial time ordering prescription [MOR78, RBN97, Yan98] or Tokuyama-Mori approach [Čáp94]. Using the Tokuyama-Mori identity instead of the Nakajima-Zwanzig identity, one gets in second-order perturbation theory for the wire-lead coupling the following equations for the population dynamics of the wire

$$\begin{aligned}\dot{\rho}_S(t) &= -i\mathcal{L}_S(t)\rho_S(t) \\ &\quad - \sum_{xx'}[K_x,\ \Lambda_{xx'}(t)\rho_S(t) - \rho_S(t)\widehat{\Lambda}_{xx'}(t)] \\ &\quad - \sum_{n}^{N}[K_n,\ \Theta_n(t)\rho_S(t) - \rho_S(t)\widehat{\Theta}_n(t)]\end{aligned} \tag{4.50}$$

with the modified corresponding auxiliary operators for the wire-lead coupling

$$\Lambda_{xx'}(t) = \int_{t_0}^{t} \mathrm{d}t' C_{xx'}(t-t') U_S(t,t') K_{x'} \tag{4.51}$$

$$\widehat{\Lambda}_{xx'}(t) = \int_{t_0}^{t} \mathrm{d}t' C^*_{x'x}(t-t') U_S(t,t') K_{x'} \tag{4.52}$$

and for the coupling to the phonon bath

$$\Theta_n(t) = \int_{t_0}^{t} \mathrm{d}t' C(t-t')\, U_S(t,t') K_n \tag{4.53}$$

$$\widehat{\Theta}_n(t) = \int_{t_0}^{t} \mathrm{d}t' C(t-t')\, U_S(t,t') K_n. \tag{4.54}$$

One can also derive these equations by just applying the substitution

$$\rho(t') = U_S^{\dagger}(t,t')\rho(t) \tag{4.55}$$

to the corresponding set of TNL equations [Kle04] neglecting the influence of dissipation during the time propagation of the density operator within the integral. Formally, this is in contradiction to the definition of a non-Markovian process which requires to respect memory effects in the relaxation process. It depends strongly on the coupling parameters whether TNL or TL is favorable [Kle04, YX05]. Within the parameter regime important for the our numerical investigations, TL and TNL calculations show almost identical results.

The derivation of Eqs. (4.15, 4.29, 4.30, 4.32, 4.46, 4.47) (as well as the related TL equations) is the first major formal result of this thesis. It was especially difficult to derive a correct decomposition for the spectral density of the electron reservoir and to find an operator basis, which accounts for the orbital description of the wire as well as for the algebraic structure of the coupling terms.

In the next chapter, this theoretical groundwork is utilized in order to derive a current equation for the system.

Chapter 5

THE ELECTRICAL CURRENT

5.1 The current equation

An intuitive approach to the electric current equation is to consider the rate of change of the number of electrons, with elementary charge e, inside the lead. This can be formulated utilizing a density matrix approach [BS93, LKHN02, LLY+05, ON05, LIH02, LCKH03, LKHN03, LKMH04, CKH04, KLH05, KCS+04] as

$$I_l(t) = e\frac{\mathrm{d}}{\mathrm{d}t}\mathrm{tr}\,\{N_l\rho(t)\}\,. \tag{5.1}$$

Here, $N_l = \sum_q c_q^\dagger c_q$ denotes the electron number operator of the left fermionic lead. The summation is taken over all reservoir modes q. Similar to the last sections, all calculations refer to the left lead only but are also valid for the right lead by adding the corresponding terms to the final set of differential equations. The trace and the density operator ρ in Eq. (5.1) are defined in the Hilbert space of the full system consisting of wire plus electron reservoir. Applying the Liouville equation (2.10) for the time derivative of the density matrix and using the cyclic properties of the trace results in

$$I_l(t) = -ie\,\mathrm{tr}\,\{[N_l, H(t)]\rho(t)\}\,. \tag{5.2}$$

By using the properties of the electron creation and annihilation operators it can be shown that the only non-vanishing commutator of N_l with the Hamiltonian (3.1) is given by the coupling term

$$[N_l, H(t)] = [N_l, H_{SR}]. \tag{5.3}$$

Evaluating Eq. (5.3) and making extensive use of Eqs. (3.3, 3.4) leads to

$$I_l(t) = -e\sum_q \mathrm{tr}\left\{\left(V_q^* c_q^\dagger c_q c_q^\dagger c_1 - V_q c_1^\dagger c_q c_q^\dagger c_q\right)\rho(t)\right\} \tag{5.4}$$

which can be further simplified to

$$I_l(t) = -e\sum_q \mathrm{tr}\left\{V_q^* c_1 c_q^\dagger \rho(t) - V_q c_1^\dagger c_q \rho(t)\right\}. \tag{5.5}$$

The second term is the conjugate of the first one and we can therefore execute the subtraction. This results in

$$I_l(t) = -2e \sum_q \mathrm{Im}\,\mathrm{tr}\left\{V_q c_1^\dagger c_q \rho(t)\right\}. \tag{5.6}$$

Because the trace is invariant under a transformation into the interaction picture, we can transform Eq. (5.6) into

$$I_l(t) = -2e \sum_q \mathrm{Im}\,\mathrm{tr}\left\{V_q \tilde{c}_1^\dagger(t)\tilde{c}_q(t)\tilde{\rho}(t)\right\}, \tag{5.7}$$

by employing $\tilde{A}(t) = U_S(t,t_0)A$ for an arbitrary operator A defined in the Hilbert space of the full system.

Switching into the interaction picture and inserting the integrated form of the Liouville equation for the full density operator in the interaction picture

$$\tilde{\rho}(t) = \tilde{\rho}(t_0) - i\int_{t_0}^{t} \mathrm{d}t'\,[\tilde{H}_{SR}(t'), \tilde{\rho}(t')], \tag{5.8}$$

into the corresponding Liouville equation provides another method to derive a quantum master equation [LKHN02, LLY+05, LIH02, LCKH03, LKHN03, LKMH04]. It also respects the coupling to the environment in second-order perturbation theory and maintains the important phase information between the operators in the trace. Applying Eq. (5.8) to Eq. (5.7) leads to

$$I_l(t) = 2e\,\mathrm{Re}\sum_q V_q\,\mathrm{tr}\left\{\tilde{c}_1^\dagger(t)\tilde{c}_q(t)\int_{t_0}^{t}\mathrm{d}t'\,[\tilde{H}_{SR}(t'),\,\tilde{\rho}(t')]\right\}. \tag{5.9}$$

Solving the commutator and arranging the operators with respect to system and reservoir results in

$$\begin{aligned} I_l(t) = 2e\,\mathrm{Re}\sum_q |V_q|^2 \int_{t_0}^{t}\mathrm{d}t'\,\mathrm{tr}\Big\{&\tilde{c}_1^\dagger(t)\tilde{c}_1(t')\tilde{c}_q(t)\tilde{c}_q^\dagger(t')\tilde{\rho}(t') \\ &-\tilde{c}_1(t')\tilde{c}_1^\dagger(t)\tilde{c}_q^\dagger(t')\tilde{c}_q(t)\tilde{\rho}(t')\Big\}. \end{aligned} \tag{5.10}$$

One can separate the full density operator (2.12) and collect the reservoir operators by comparing the resulting terms with the definition of the reservoir correlation functions (4.9). Thus, one finds

$$C_{12}(t-t') = \sum_q |V_q|^2\,\mathrm{tr}_R\left\{\tilde{c}_q(t)c_q^\dagger(t')\rho_R\right\} \tag{5.11}$$

$$C_{21}^*(t-t') = \sum_q |V_q|^2\,\mathrm{tr}_R\left\{c_q^\dagger(t')\tilde{c}_q(t)\rho_R\right\}. \tag{5.12}$$

A backward transformation into the Schrödinger picture proves the equality of Eqs. (5.11, 5.12) with definition (4.9). The current equation therefore simplifies to

$$I_l(t) = 2e\,\mathrm{Re}\int_{t_0}^{t} \mathrm{d}t' \left(\mathrm{tr_S}\left\{\tilde{c}_1^\dagger(t)\tilde{c}_1(t')\tilde{\rho}_S(t')\right\} C_{12}(t-t') \right. \\ \left. -\mathrm{tr_S}\left\{\tilde{c}_1(t')\tilde{c}_1^\dagger(t)\tilde{\rho}_S(t')\right\} C_{21}^*(t-t')\right). \tag{5.13}$$

The current information is partly contained in the temporal phase relation between the annihilation, creation and density operators and can be incorporated into a single time evolution operator U_S, defined in the Hilbert space of the relevant system. This corresponds to a transformation into the Schrödinger picture. After using the cyclic properties of the trace, we can write Eq. (5.13) as

$$I_l(t) = 2e\,\mathrm{Re}\left(\mathrm{tr_S}\left\{c_1^\dagger \int_{t_0}^{t} \mathrm{d}t'\, U_S^\dagger(t',t)\, c_1 \rho_S(t')\right\} C_{12}(t-t') \right. \\ \left. -\mathrm{tr_S}\left\{c_1^\dagger \int_{t_0}^{t} \mathrm{d}t'\, U_S^\dagger(t',t)\, \rho_S(t') c_1\right\} C_{21}^*(t-t')\right). \tag{5.14}$$

Performing the steps leading from Eq. (5.6) to Eq. (5.14) in the Schrödinger picture (non-interaction picture) would lead to a physically inconsistent dissipation term. This is due to the fact, that the internal dynamics governed by the wire Hamiltonian is lost when the Schrödinger picture counterpart of Eq. (5.8) is applied to Eq. (5.7) (notice Eq. (5.3)). Within the interaction picture, the information of the internal dynamics of the wire is contained in the phase information of the operators and therefore maintained. It appears again in form of the time evolution operator $U_S(t',t)$ in Eq. (5.14). One should also notice, that we assume (Eq. (5.11), (5.11)) that the electron reservoir stays in thermal equilibrium in order to trace out the reservoir modes. This is in contradiction to the initial ansatz (5.1), where we measured the current by counting the change of the electron number in the lead. The approach survives this contradiction due the properties of the interaction picture. One should imagine the presented computations as an attempt to install an electron counter around the reservoir instead of counting the electrons inside the reservoir.

The integrals in Eq. (5.14) have the same structure as the auxiliary density matrices defined in the last section and can be expressed in terms of $\Lambda_{12}(t)$ and $\widehat{\Lambda}_{12}(t)$. Thus, we get the final equation for the time-dependent current between the left lead and the first site of the wire

$$I_l(t) = 2e\,\mathrm{Re}\left(\mathrm{tr}_S\left\{c_1^\dagger \Lambda_{12}(t) - c_1^\dagger \widehat{\Lambda}_{12}(t)\right\}\right). \tag{5.15}$$

Similar to the master equation (4.15), all the information about the interaction of the system with the reservoir is stored in the time-dependent auxiliary matrices

(4.13) and (4.14) weighting the corresponding system operator. It is valid within the framework of assumptions we have to make in order to derive Eq. (4.15) and allows to compute the time resolved current in systems with arbitrary time-dependence. The EOM for the required auxiliary operators are already given by Eq. (4.29, 4.30). Thus, a complete set of differential equations consisting of Eqs. (4.29, 4.30, 4.46, 4.47), the master equation (4.15) together with the phonon bath dissipation term (4.36) and the current equation (5.15) provides a formalism to compute the current and the population dynamics for a wide range of systems. The same set of equations has to be applied to the last site of the wire as well to describe a wire enclosed by two leads, as shown in Fig. 3.1. Furthermore, the potentiality of the formalism to define any desired number of leads makes it possible to realize driven current switches with an arbitrarily complicated configuration.

The TL analog of Eq. (5.15) can be derived by applying the substitution (4.55) and reads

$$I_l(t) = 2e\,\mathrm{Re}\left(\mathrm{tr}_S\left\{c_1^\dagger \Lambda_{12}(t)\rho_S(t) - c_1^\dagger \rho_S(t)\widehat{\Lambda}_{12}(t)\right\}\right). \tag{5.16}$$

In section 6.2, we present a short numerical comparison of TL and TNL current equations.

5.2 The current operator

Without simplifying the substraction in Eq. (5.5) and performing the steps leading from Eq. (5.6) to Eq. (5.15), we derive the current equation

$$I_l(t) = e\,\mathrm{tr}_S\left\{c_1^\dagger \Lambda_{12}(t) - c_1^\dagger \widehat{\Lambda}_{12}(t) + c_1 \widehat{\Lambda}_{21}(t) - c_1 \Lambda_{21}(t)\right\} \tag{5.17}$$

which also includes its conjugate part within the trace. This conjugate part is not interesting for the expectation value of the current and Eq. (5.17) is numerically not as effective as Eqs. (5.15, 5.16) since it requires twice as many matrix operations. But we need it to derive a Hermitian current operator. First we have to transform Eq. (5.17) into a TL form by applying substitution (4.55)

$$I_l(t) = e\,\mathrm{tr}_S\left\{c_1^\dagger \Lambda_{12}(t)\rho_S(t) - c_1^\dagger \rho_S(t)\widehat{\Lambda}_{12}(t) + c_1 \Lambda_{21}(t)\rho_S(t) - c_1 \rho_S(t)\widehat{\Lambda}_{21}(t)\right\}. \tag{5.18}$$

By rearranging the operators using the cyclic properties of the trace, we can extract a time-dependent current operator for the electronic lead in the TL approach. Thus, a generic expression

$$I_l(t) = e\,\mathrm{tr}_S\left\{\mathcal{I}_l(t)\rho(t)\right\}, \tag{5.19}$$

for the dissipative current is derived by defining the current operator $\mathcal{I}_l(t)$

$$\mathcal{I}_l(t) = c_1^\dagger \Lambda_{12}(t) - \widehat{\Lambda}_{12}(t)c_1^\dagger + \widehat{\Lambda}_{21}(t)c_1 - c_1 \Lambda_{21}(t). \tag{5.20}$$

This time-dependent operator consists of the same auxiliary operators as the dissipation term of the TL master equation (4.50) and is therefore propagated along with the reduced density matrix. One could also derive the current operator by just symmetrizing the expression in the trace of Eq. (5.16) but we want to point out the relation to the dissipation term of the master equation (4.50). The existence of a generic Hermitian current operator for the electron transfer in our system enables a more formal treatment of the current within the operator framework of quantum mechanics. This important step is the foundation of the derivation of an optimal control formalism for the molecular wire.

Chapter 6

NUMERICAL EXAMPLES

The systems depicted in Fig. 3.1 and Fig. 3.2 represent simple configurations which already allow studies of a variety of transport phenomena. All numerical results are expressed in terms of the tight-binding hopping parameter Δ, where $\Delta = 0.1$ eV is a reasonable value for molecular systems [LKHN02, LIH02, LCKH03, LKHN03, LKMH04, CKH04, KLH05]. Despite the fact that it would be possible, we do not simulate a realistic coupling spectrum between the leads and the wire and restrict our coupling spectrum to a single Lorentzian. For example, a realistic gold s-band would be a superposition of different Lorentzians forming a variety of band edges. Taking only one Lorentzian into account corresponds to a rough approximation of only one band edge, but this makes the system and the underlying processes easier to understand. We apply this restriction also to the phonon bath spectral density.

Due to the weak coupling requirement, the spectral density of the reservoir should be about one order smaller than the internal dynamics. Thus the peak of the Lorentzian $J(\omega)$ is set to 0.1Δ, which is guaranteed by the condition

$$p_1 = 0.1 \left(4\Delta\Omega_1\Gamma_1^2\right). \tag{6.1}$$

Reasonable values for the bandwith parameters Γ_k are in the region of 10 eV. With the chosen energy settings, an unit time in the system corresponds to 0.66 fs in real time what enables one to resolve time-dependent effects on a femtosecond scale. The resulting current unit can be extracted from Eq. (5.15) and is equal to a macroscopic value of $1[I] = [\frac{e}{[t]}] = 2.43 * 10^{-4}$ A. A detailed discussion of the relation between the applied numerical unit system and macroscopic values is given in Appendix A. The computations in sections 6.1 6.2, 6.3, 6.6 and 6.7 are realized without applying a vibrational coupling to the wire, while the sections 6.4, 6.5 and 6.6 utilize coupling to electron reservoirs and to a phonon bath.

6.1 The transient oscillation of the undriven wire

The equilibrium condition of the on-site population of the wire in the absence of a second lead is determined by the Fermi function n_F taken at the on-site energy E_i, namely

$$n_i = \mathrm{tr}(c_i^\dagger c_i \rho_S(t)) = n_F(E_i - E_F). \tag{6.2}$$

In this particular case, the current drops to zero after the wire has reached its equilibrium level, simply due to the lack of a closed electrical circuit. The situation is more interesting in the case where two leads are coupled to the wire, as it is shown in Fig. 3.1. For instance, Fig. 6.1 shows a situation for a wire consisting of two sites, in which the wire states at time zero are unoccupied. The equilibrium state is reached after a relaxation time that mostly depends on the wire-lead coupling strength.

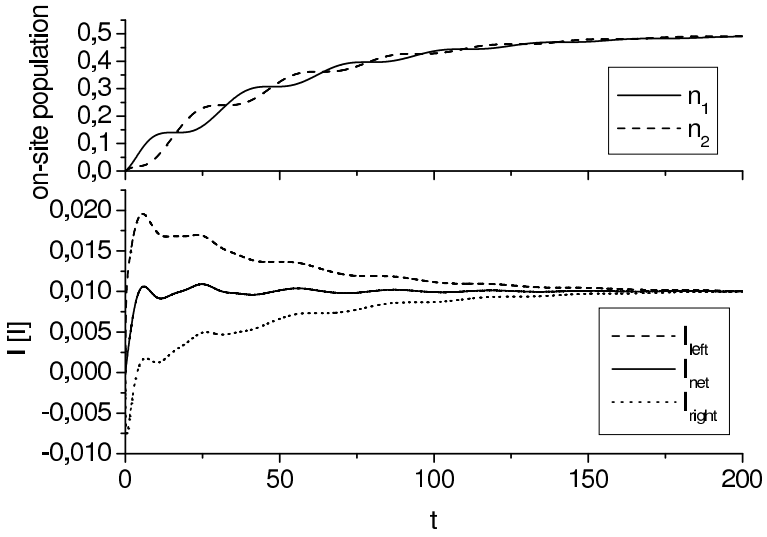

Figure 6.1: Upper panel: population dynamics measured by $n_i = \mathrm{tr}(c_i^\dagger c_i \rho_S(t))$ $(i = 1, 2)$ for the undriven two site system as a function of time t starting with unoccupied wire states. The applied DC voltage is realized by a difference between the left and the right Fermi energy of $E_{F,l} - E_{F,r} = 10\Delta$. The on-site energies of the wire are aligned and centered between the left and the right Fermi energy $E_1 = E_2 = E_{F,r} + 5\Delta = E_{F,l} - 5\Delta$. Bottom panel: the corresponding currents flowing from the left lead into the first site I_{left}, from the right site into the right lead I_{right} and the net current $I_{net} = (I_{left} + I_{right})/2$.

While the number of electrons in the relevant system is not constant in time, the trace of the reduced density operator is conserved and normalized. A bias voltage

on the system can be simulated by setting a difference between the left and right Fermi energy, here $E_{F,l} - E_{F,r} = 10\Delta$. Since we set the on-site energies to $E_1 = E_2$ and apply a weak coupling scheme where the internal dynamics of the inner system is about one order faster than the electron transfer between the leads and the wire, a spatial drop of the population within the wire in its equilibrium state cannot be observed in the upper panel of Fig. 6.1.

The equilibrium population of the entire wire is determined by the average over the expectation values of the left and right sites, which is given by

$$\mathrm{tr}\left(c_1^\dagger c_1 \rho_S(t)\right) \approx \mathrm{tr}\left(c_2^\dagger c_2 \rho_S(t)\right) \approx \frac{n_F(E_1 - E_{F,l}) + n_F(E_2 - E_{F,r})}{2} \tag{6.3}$$

if the spectral densities of both leads, i.e. their coupling to the wire, are the same. The transient oscillations of the corresponding directed net current decay and a constant equilibrium value is reached, when the relaxation process is over. The upper bound for the net current is determined by the small wire-lead coupling strength, namely the spectral function $J_R(\omega)$ with its maximum value of 0.1Δ.

6.2 Comparison of time-local and time-nonlocal approach

Fig. 6.2 shows a comparison of TL and TNL approaches for different spectral densities. The wire states are initially unoccupied and electrons migrate from the leads into the wire sites, depicted in the middle panel of Fig. 6.2. Despite both on-site energies have been chosen equal to the Fermi levels $E_1 = E_2 = E_{F,l} - 5\Delta = E_{F,r} + 5\Delta$, the equilibrium occupation value for both sites is given by $n_1 \approx n_2 \approx 0.5$ in the case of a weak wire lead coupling. For larger coupling terms (with respect to second-order perturbation), for instance $p_1 = 22.5\Delta$, one observes a spatial drop of the population in the wire $n_1 > n_2$. For a broad spectral band, i.e. large Γ_1, TL and TNL calculations show a good agreement for the different coupling strengths. However, a shift between the equilibrium values of the two approaches arises for very narrow bands and relatively strong wire-lead coupling for the population dynamics and the corresponding current, depicted in the upper panel of Fig. 6.2. This deviation can be explained with different higher order terms of the TL and the TNL approach [Kle04], which become more important for larger coupling strengths. At $100 < t < 110$, we apply a rectangular pulse with amplitude $A = 10\Delta$ to the system to check whether the TL and TNL approximations agree in the different parameter regimes in their dynamical behavior. In this highly dynamical situation, both approaches show a good agreement even in the critical parameter regimes.

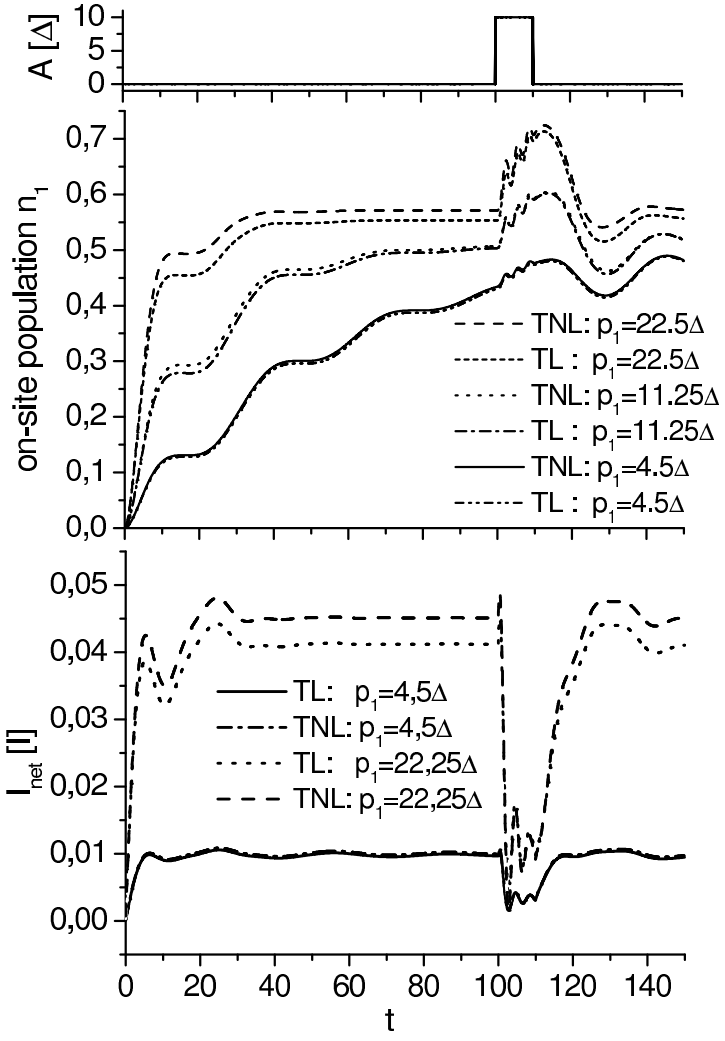

Figure 6.2: A comparison of TNL and TL calculations for a small band width parameter $\Gamma_1 = 7.5\Delta$. The upper panel shows the applied rectangular pulse with an amplitude of $A_0 = 10\Delta$ which influences the site populations of the wire which are shown in the lower panel. The difference between TL and TNL populations becomes more evident for stronger lead-wire couplings adjusted by the parameter p_1 in the spectral decomposition of $J_R(\omega)$. The on-site energies and the left and right Fermi energies are aligned $E_1 = E_2 = E_{F,l} + 5\Delta = E_{F,r} - 5\Delta$.

6.3 Time-dependent electron reservoirs

Time-dependent electron reservoirs in molecular systems can be modelled within the Floquet theory by applying a gauge transformation on the wire Hamiltonian [KLH05] or by using a source-Redfield [ON05] equation. Despite the fact that we initially assumed that the lead Hamiltonian is time-independent, the formalism allows one to treat time-dependent lead Hamiltonians as well by simply considering time-dependent coefficients for the correlation functions $C(t) = \sum_k a_k(t) e^{\gamma_k(t)t}$, in the case of the TL theory, and a time derivative given by

$$\frac{\mathrm{d}}{\mathrm{d}t} C(t) = \sum_k^{m+m'} a_k(t) e^{\gamma_k(t)t} \left(\gamma_k(t) + \dot{\gamma}_k(t)t\right) + \sum_k^{m+m'} \dot{a}_k(t) e^{\gamma_k(t)t}. \tag{6.4}$$

To get the required form $\dot{C}(t) = \gamma_k(t) C(t)$ which is necessary to derive differential equations for Eqs. (4.13, 4.14), we have to assume that

$$|\dot{a}_k(t)| \ll |a_k(t)\gamma_k(t)|, \tag{6.5}$$

$$|e^{\gamma_k(t)t} \dot{\gamma}_k(t) t| \ll |e^{\gamma_k(t)t} \gamma_k(t)|, \tag{6.6}$$

for all times t not negligible in the time integration of the auxiliary operators in Eqs. (4.13, 4.14). In general, this assumption corresponds to the statement that the lead dynamics is sufficiently slower than the lead-wire coupling dynamics. The lead-wire coupling can be influenced by a variation of the chemical potential of the electron distribution in the leads, by changing the parameters Ω_k, Γ_k, p_k of the spectral decomposition, or both. A change in the chemical potential and keeping the spectral function unchanged would correspond to a charging process. Shifting the spectral density, i.e. increasing or decreasing the Ω_k parameters, and the chemical potential by the same value describes a total change of the electrostatic potential without an alteration of the population in the leads.

In the present work, we restrict ourselves to a time-periodic modulation of the difference between the chemical potentials of the left and right lead

$$E_{F,r} - E_{F,l} = V_0 \sin(\omega_V t), \tag{6.7}$$

thereby approximating an AC voltage on the leads with amplitude V_0. In this special case, the quality of the approximation of slow dynamics can be determined considering the general time dependence of the coefficients given by Eqs. (4.25, 4.26) as

$$|a_k(t)| \sim |n_F\left(E_F\left(t\right)\right)| \tag{6.8}$$

for the FFR terms with the corresponding time-independent exponents γ_k. Therefore, the time derivative becomes

$$|\dot{a}_k(t)| \sim |n_F^2\left(E_F\left(t\right)\right) \beta \dot{E}_F(t)| \sim |\frac{V_0\, \omega_V}{T} \cos\left(\omega_V t\right) n_F^2\left(E_F\left(t\right)\right)| \tag{6.9}$$

and conditions (6.5, 6.6) are justified if

$$|\frac{V_0\,\omega_V}{T}| \ll 1. \tag{6.10}$$

Regarding the FFR terms, the relevant time-dependent coefficients are

$$\gamma_k(t) = -(2\pi k + \pi)T + iE_F(t) \tag{6.11}$$

and

$$|a_k(t)| = |2TJ(\nu_k)| \tag{6.12}$$

for $k = 1 \ldots m'$. It can be shown that conditions (6.5, 6.6) are fulfilled if

$$\frac{V_0\,\omega_V}{(\pi + 2\pi k)T} \ll 1 \tag{6.13}$$

which complies with the condition for the non-FFR coefficients (6.10). A disregard of the conditions (6.5, 6.6) would cause additional fast oscillations of the current during those times in which the AC voltage changes rapidly. The AC voltage causes an AC in the system, both shown in Fig. 6.3, that follows the driving voltage. For large voltage amplitudes V_0 a finite cut-off appears due to a bottle neck of the system given by its weak coupling to the electronic leads.

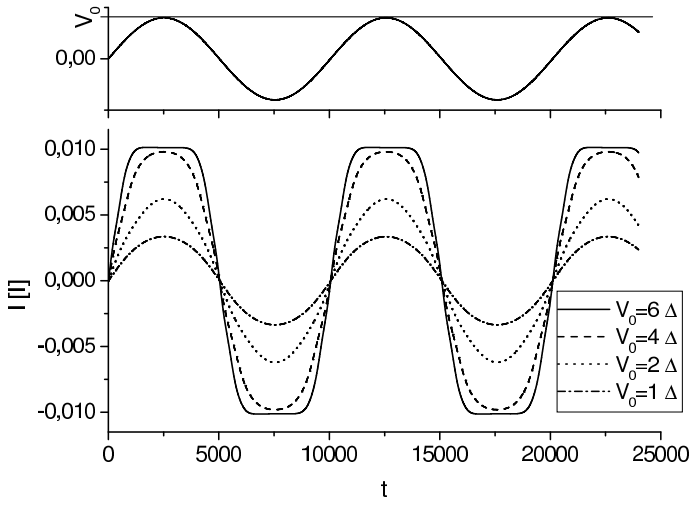

Figure 6.3: The alternating voltage (upper panel) with amplitude V_0 and frequency $\omega_V = \Delta/160$ drives an AC (bottom panel) between the left and the right lead through an wire consisting of five sites. A current cut-off appears for large AC voltages, since the wire-lead coupling is weak.

6.4 Coherent destruction of tunneling

Coherent destruction of tunneling (CDT) [LCKH03, LKMH04, CKH04, GDJH91, KCS+04] is a well understood quantum mechanical effect where an external periodic driving field of the form

$$A(t) = A_0 \sin(\omega_d t) \tag{6.14}$$

yielding an asymmetric potential $U_n(t) = \frac{A(t)}{2}(\delta_{1n} - \delta_{2n})$ in Eq. (3.5) can suppress the time-averaged current in the field-driven two-site system. The current completely breaks down if the ratio of the field parameters $A_0/\hbar\omega_d$ is equal to a zero of the Bessel function J_0 (e.g. 2.405, 5.520, 8.654, ...), a condition that holds for isolated quantum systems as well as for open systems [LCKH03, LKMH04, KCS+04, CKH04].

This is a simple but nontrivial system for a time-dependent conduction formalism and we extend the results of former calculations which applied the wide-band approximation [LCKH03, LKMH04, KCS+04, CKH04] to finite band effects by using a spectral decomposition. The finite width of the decomposed spectral density (4.24) causes an additional decay of the current with increasing amplitude since the coupling strength between the lead and the corresponding site decreases when the on-site energy of the coupled site is driven to the edges of the Lorentzian during the oscillation generated by the external field $A(t)$. Naturally, this effect becomes more dominant for a smaller bandwidth parameter Γ_1, shown in Fig. 6.4. The time-averaged current shows the predicted breakdowns at the zeros of J_0. The amplitude A_0 of the applied electrical field is here given in dimensions of $[\Delta]$ which corresponds to field strengths of about $10^8 \frac{\mathrm{V}}{\mathrm{cm}}$ by assuming atomar distances of 1 Å. The driving frequency is set to $\omega_d = 10\Delta$ which is in the low energy branch of infrared light. Here the bias voltage is set to $E_{F,l} - E_{F,r} = 60\Delta = 6$ eV.

Similar to recent studies [LKMH04], we also apply an additional vibrational coupling to the driven wire. The strength of the spectral density of the phonon bath (4.24) determines the transport regime in the wire. In its absence we see fully coherent transport regime which gradually becomes a sequential hopping regime for larger spectral densities. This can be explained in the framework of quantum mechanics by a suppression of the coherences due to the vibrational environment.

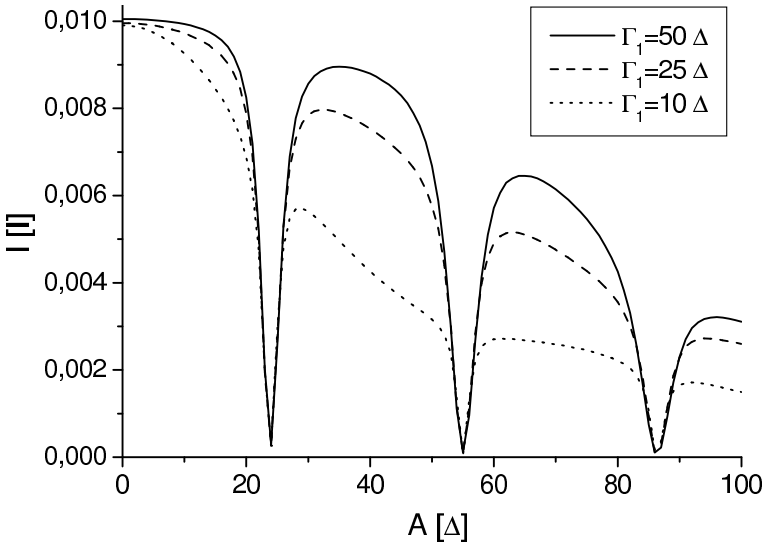

Figure 6.4: The time-averaged current for the periodically driven two-site system as a function of the amplitude for different bandwith parameters Γ_1. The frequency of the external field is $\omega_d = 10\Delta$. The applied bias voltage is 60Δ. The Fermi energies $E_{F,r} = \Omega_1 - 30\Delta$, $E_{F,l} = \Omega_1 + 30\Delta$ and the on-site energies $E_1 = E_2 = \Omega_1$ are set in relation to the parameter Ω_1 of the spectral density.

Thus, the requirement for CDT, namely coherent transport, vanishes and the supressions in Fig. 6.4 are smoothed, as it is shown in Fig. 6.5. Unlike reference [LKMH04], we also observe a significant widening of the supressions, what is probably due to a different parameter regime. For instance, a stronger wire-lead coupling is applied here. Also, the absence of the wide band approximation in our calculations can cause an additional variation in comparison to reference [LKMH04]. The numerical example demonstrates the importance of the vibrational coupling to the transport and the applicability of the developed method.

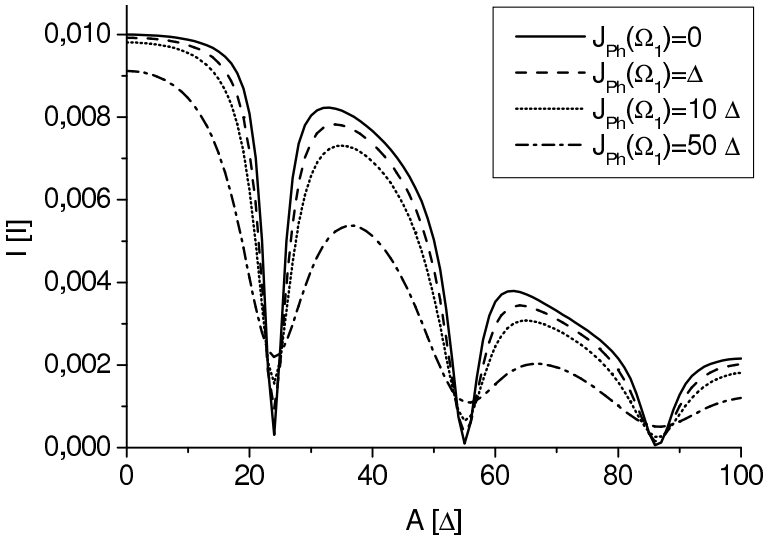

Figure 6.5: Same system as in Fig. 6.4 but the wire is additionally subject to a vibrational coupling. The bandwidth parameter of the electron reservoirs is set to $\Gamma_1 = 50\Delta$ and the bias voltage is given by 40Δ. The reduction of current due to CDT become less distinct for larger phonon bath coupling strengths given by the maximum of the phonon bath spectral density (4.24).

6.5 Vibrationally driven current

In this section, we want to discuss shortly an effect caused by the thermal coupling to the phonon bath. We employ a two site wire as depicted in Fig. 6.6. Both leads are at the same Fermi energy and the on-site energy of the left site is fixed at a higher value than the left one, $U_{12} = E_1 - E_2$ and $E_F = (E_1 + E_2)/2$, giving the wire an asymmetric configuration. The Fermi energy is also equal to the maximum of the spectral density $\Omega_1 = E_F$. The temperature is set to $k_B T = 0.5\Delta$.

Fig. 6.7 depicts the net current in as it is shown in Fig. 6.6 for $U_{12} = \Delta$. From the initial time until $t = 400$, the system is propagated without influence from the phonon bath and one observes the typical relaxation behavior as it is described in section 6.1. Due to the absence of a bias voltage, the equilibrium net current is zero. Then the thermal bath is switched on and the current changes to another equilibrium value. The appearance of this current can be explained in terms of different site occupation values in thermal equilibrium.

In the given case, the equilibrium values of the sites are determined by the Fermi function when the system coupled to the electron reservoirs only. Thus, $n_1 = n_F(E_1 - E_F) \approx 0.269$ and $n_2 \approx 0.731$. If the phonon bath applys only to the

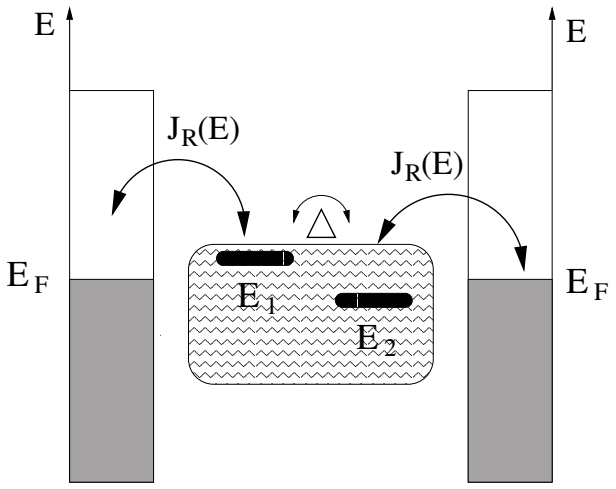

Figure 6.6: A two site wire is coupled to two electron reservoirs and is subject to a vibrational environment, but no laser field is applied. There is no bias voltage applied to the wire; both reservoirs are at the same Fermi energy E_F. The left site is at a higher energy level than the right site and $E_F = (E_1 + E_2)/2$. The difference between the on-site energies is $U_{12} = E_1 - E_2$.

system, the equilibrium occupation values of the sites are given by Bose statistics, namely

$$n_1 = \frac{\exp(-\beta E_1)}{Z} \approx 0.119$$

and $n_2 \approx 0.881$. Z is the partition function.

Thus, we have an additional relaxation from the higher state to the lower state and due to the spatial configurations of our sites, this relaxation causes a directed current. This different scaling behavior also explains the dependency of the related current on the value of U_{12} as depicted in Fig. 6.8. An increase of the current is observed for small values before the system enters a regime in which the current decreases with increasing U_{12} again. Furthermore, the on-site energies of the wire are also in an unfavorable coupling region in relation to the leads for larger U_{12} values. The electron transfer in the given system realizes an energy transfer between the left lead and phonon bath and right lead in favor of the two latter ones.

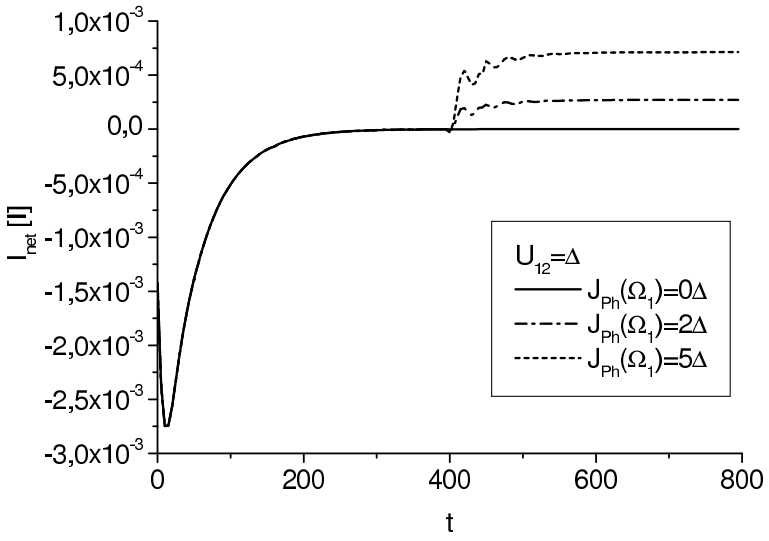

Figure 6.7: The net current through the system depicted in Fig. 6.6. After the system has reached its equilibrium, the coupling to the phonon bath is switched on at $t = 400$. The resulting final net current depends on the value of the spectral density of the phonon bath $J_{Ph}(\Omega_1)$. The temperature is set to $k_B T = 0.5\Delta$. The bandwidth of the electron reservoirs is $\Gamma_1 = 30\Delta$.

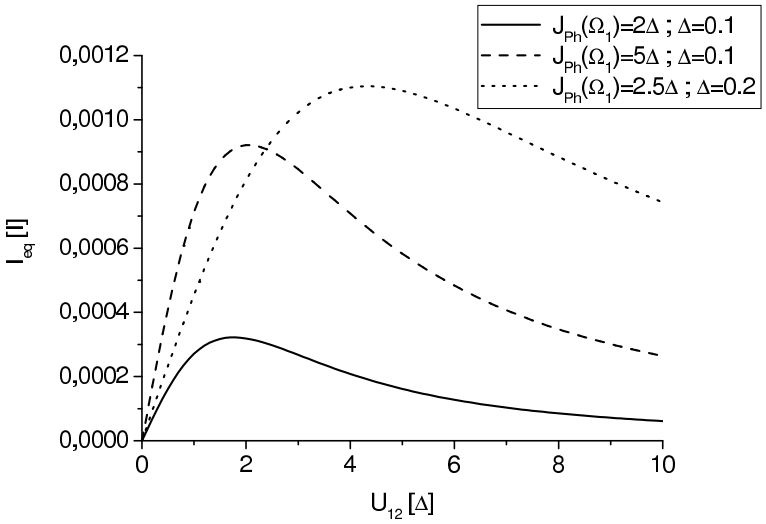

Figure 6.8: The dependence of the current driven by the phonon bath on the value of U_{12} for different phonon bath spectral densities $J_{Ph}(\Omega_1)$.

The effect is steady since the on-site energies of the wire and the temperature and Fermi levels of the bath and the reservoirs are fixed in an artificial way. In real systems, the current would stop once a new equilibrium value is reached. Thus one would have to apply another dynamical driving source in the wire in order to maintain the current.

A conclusive proof for the energy transfer in the system could be made by utilizing an energy flow operator in analogy to our current operator (5.20). It should be possible to derive such an operator within the provided theoretical network by following the guideline presented in section 5.1. A measure of the energy flow from the phonon bath into the system and vice versa would provide another powerful tool to understand the transport in mesoscopic systems. Especially effects like current induced light emission [GN] could be studied in highly dynamical situations. This project will be subject to further investigations.

6.6 I-V characteristics

An important property of the system of interest is its current-voltage characteristic since this quantity is experimentally approachable and also provides access to important intrinsic information. In contrast to I-V calculations employing DFT methods to simulate realistic molecules, the simple tunneling Hamiltonian utilized in this section does not contain any information related to certain molecules. One of the basic ideas of molecular electronics [AR74] is the construction of current rectifiers. The required asymmetric transport properties can already be simulated with the simple configurations discussed in previous sections. Furthermore, an I-V characteristic gives one a better understanding of the wire-lead contact which is here realized in second-order pertubation theory.

Fig. 6.9 shows the I-V curve for a 4-site tight-binding Hamiltonian for different energy configurations and temperatures. The parameters employed in the calculation are as follows. The bandwidth of the spectral density (4.24) is set to $\Gamma = 25\Delta$ and the position of the center Ω_1 of the Lorentzian is equal to the average of the on-site energies. Both leads are characterized by the same spectral density. We chose a higher setting for the temperature, e.g. $k_BT = \Delta$, in order to get a better resolution of the different regimes. At $k_BT = 0.25\Delta$, the I-V spectrum would be almost a step function in the scale used in Fig. 6.9. We also employed only a single Lorentzian to represent the spectral density of the phonon bath. The voltage is simulated by just setting a difference between the left and the right Fermi energy $V = E_{Fl} - E_{Fr}$ such that $E_{F,l}(V) = E_{F,l}(V = 0) + V/2$ and $E_{F,r}(V) = E_{F,r}(V = 0) - V/2$. The average of all on-site energies equals the Fermi energy for $V = 0$.

The upper panel of Fig. 6.9 depicts the I-V function for an symmetric Hamiltonian where all on-site energies are equal $E_1 = E_2 = E_3 = E_4$ and no phonon bath

is applied. Therefore, one observes a symmetric I-V characteristic which becomes flatter for higher temperatures. At small bias voltages, the system operates within a linear response regime before it enters a cut-off regime caused by the finite wire-lead coupling at higher voltages. Increasing the bias voltage does not affect the value of the equilibrium current within the cut-off regime.

The flattening of the I-V function in the upper panel of Fig. 6.9 can be explained by considering that the occupation of the electronic leads is determined by the Fermi function which becomes smoother for larger temperatures. Thus, the occupation level difference between the left and the right lead becomes less distinct for higher temperatures, which decreases the current for small voltages.

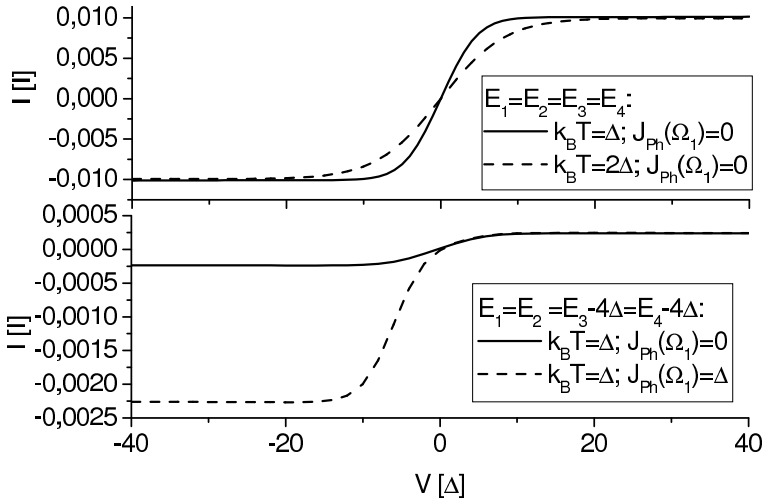

Figure 6.9: Upper panel: I-V characteristic for different temperatures of the system depicted in Fig. 3.1 employing a symmetric wire, $E_1 = E_2 = E_3 = E_4$, consisting of 4 sites. No phonon bath is applied. Bottom panel: An asymmetric system with the on-site energy configuration $E_1 = E_2 = E_3 - 4\Delta = E_4 - 4\Delta$. One observes an asymmetric transport characteristic in the presences of a vibrational environment.

The bottom panel of Fig. 6.9 depicts a 4-site tight-binding Hamiltonian with an asymmetric energy setting, viz. $E_1 = E_2 = E_3 - 4\Delta = E_4 - 4\Delta$. We employ this configuration in order to study asymmetric transport properties. With the chosen energy settings, one finds that the I-V curve is still symmetric in the absence of a dissipative phonon bath where we have coherent transport. Here, different transport channels, determined through the eigenenergies of the Hamiltonian, realize the transport and the asymmetry is not reflected in the transport behavior. Since the on-site energies are not equal to the position of the maximum of the spectral

density $E_1 = \Omega_1 - 2\Delta$ and $E_4 = \Omega_1 + 2\Delta$, the coupling between the leads and the wire is weaker than in the case where $E_1 = E_4 = \Omega_1$ (upper panel of Fig. 6.9) and one observes smaller currents in the bottom panel of Fig. 6.9.

The situation is different if a phonon bath couples to the wire, as the dashed line in the bottom panel of Fig. 6.9 shows. In a scenario where the coherent transport is replaced by sequential hopping, the orbital asymmetry of the system becomes evident in its transport behavior. The increase of the current for negative bias voltages can be understand by the arguments provided in the discussion of section (6.5). The phonon bath causes an relaxation of the electrons from the higher energy level E_3 of site 3 to site 2 at energy $E_2 < E_3$. The relaxation process works also in the other direction but at a smaller rate.

6.7 Optical current switching

The major advantage of the derived conduction formalism, in addition to the avoidance of the wide-band limit, is the applicability to unrestricted time-dependent systems. Former CDT studies of currents in open quantum systems [LCKH03, LKMH04, KCS+04] were based on an infinite-time averaging of the currents due to the mathematical nature of the used approaches. In Fig. 6.10, we apply a finite laser pulse with a Gaussian shaped amplitude

$$A(t) = A_0 \exp\left(\frac{-(t-T)^2}{2\sigma^2}\right) \sin(\omega_d t) \tag{6.15}$$

to the asymmetric driven system described in the last subsection.

The peak amplitude of the Gaussian was set to $A_0 = 24.05\Delta$, where the CDT relation applies. This finite laser pulse causes the time-resolved current to oscillate around zero, shown in the center panel of Fig. 6.10. The situation becomes more obvious by looking at the time averaged current depicted in the bottom panel of Fig. 6.10, where the averaging was taken over three oscillations of the driving field.

The averaged current is almost suppressed during the time in which the Gaussian laser field is applied to the system and CDT is performed with a finite laser pulse. The effect is superimposed by transient oscillations because the system is under the constraint of permanently changing variables and tries to find its equilibrium state. This finite-time effect gives rise to interesting experimental realizations.

Further investigations in the next section will deal with the idea to apply the current formalism to an optimal control algorithm for time-distributed target states in order to compute more sophisticated and applicable external control fields.

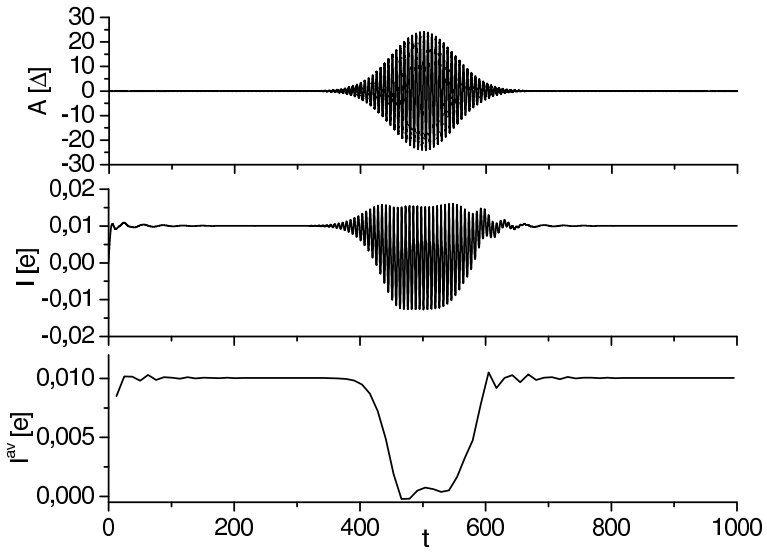

Figure 6.10: Upper panel: Gaussian excitation pulse with a peak amplitude of $A_0 = 24.05\Delta$ and a width of $\sigma^2 = 50$. It excites the time-resolved net current depicted in the middle panel. Bottom panel: The net current averaged over three periods of the fast pulse oscillation reveals a complete suppression. The on-site energies are equal $E_1 = E_2 = \Omega_1$ and centered between the left and the right Fermi energy, which define a DC voltage of $E_{F,r} - E_{F,l} = 10\Delta$.

Chapter 7

OPTIMAL CONTROL OF MOLECULAR ELECTRONICS

7.1 Optimal control theory for target states distributed in time with dissipation

In order to derive a suited control algorithm for the laser assisted transport in molecular wires, one has to merge the properties of two already existing methods and modify them in correspondence to the given constraints. Refs. [MM01, MKM02] present an optimal control algorithm for open quantum systems within the framework of the reduced density operator. In their case, the relevant system is coupled to a vibrational environment only. Their EOM is also given in terms of a quantum master equation. Here, we will follow their guideline to derive similar EOM for an optimal control algorithm related to the open system electron transfer. Furthermore, since we need to define target states distributed in time, namely a current pattern as a function of time, in order to derive a method applicable for molecular electronics, we will merge the mentioned formalism with a recent approach [KM05b, KM05a] which deals with time-distributed target states. The first step is to separate the relevant system Hamiltonian into the tight-binding part and a time-dependent dipole part according to Eq.(3.18) to write the quantum master equation (4.50) in the TL picture as

$$\dot{\rho}_S(t) = -i\mathcal{L}_{tb}\rho_S(t) - i\mathcal{L}_{\mu}(t)\rho_S(t) - D(t)\rho_S(t). \tag{7.1}$$

Eq. (3.20) gives us an expression for the Liouville dipole operator. The time-dependent dissipation operator $D(t)$ incorporates all the dissipation terms and can be determined from Eq. (4.50) as

$$D(t)\rho_S(t) = \sum_{xx'} K_x\Lambda_{xx'}(t)\rho_S(t) - K_x\rho_S(t)\widehat{\Lambda}_{xx'}(t) - \Lambda_{xx'}(t)\rho_S(t)K_x + \rho_S(t)\widehat{\Lambda}_{xx'}(t)K_x. \tag{7.2}$$

The solution of the EOM (7.1) of the reduced density operator can be formally written as

$$\rho_S(t) = U(t, t_0, A)\rho(t_0), \tag{7.3}$$

where $U(t, t_0, A)$ is the time-evolution superoperator containing the system Hamiltonian and the dissipation operator. In this section, we list the laser field amplitude

$A(t)$ explicitly as an argument of all time-evolution operators since dependencies on the control field are crucial to the following steps.

The control target is determined by the expectation value of the time-dependent target operator $\mathcal{O}(t)$. Since we want to realize time-distributed control targets, the control parameter J_0 of the control target operator $\mathcal{O}(t)$ is defined by the integral

$$J_0(A) = \int \mathrm{d}\tau \, \mathrm{tr}\{\mathcal{O}(\tau)\rho_S(\tau)\}. \tag{7.4}$$

which is a function of the laser field amplitude $A(t)$. The final purpose of the optimal control algorithm is to maximize functional (7.4). For instance, if the current operator (5.20) is applied as the control target $\mathcal{O}(t) = \mathcal{I}(t)$, we demand a control field which maximizes the current at times when the kernel of integral (7.4) has significant values. Making the replacement $\mathcal{O}(\tau) = \mathcal{O}\delta(\tau - t_f)$ leads directly to a control formalism optimizing a field to reach a certain system state at the final control time t_f [MM01, MKM02] with $J_0(t_f) = \mathrm{tr}\{(\mathcal{O}(t_f)\rho_S(t_f)\}$. The control functional is defined as

$$J(t_f, A) = J_0(A) - \frac{1}{2}\int_{t_0}^{t_f} \mathrm{d}t \, \lambda(t)A^2(t). \tag{7.5}$$

Since the intregration is performed from the initial time t_0 to the final control time t_f, the time-dependent target is also defined between initial and final time, thus $t_0 \leq \tau \leq t_f$. Here, the penalty factor of the control field (or Lagrange multiplier) $\lambda(t)$ is considered to be time-dependent to avoid sudden switch-on and switch-off behavior of the control field at the beginning and end of the propagation time of the system. In the numerical calculations, we will set $\lambda(t) = 1/\left(\lambda_1 \sin^2\left(\frac{\pi}{t_f}t\right)\right)$ with $\lambda_1 = 1$. In order to calculate the extremum of functional (7.5) under a variation of the external field $A(t)$, one has to set the corresponding functional derivative to zero:

$$\frac{\delta J(t_f, A)}{\delta A(t)} = 0 = \frac{\delta J_0(A)}{\delta A(t)} - \frac{1}{2}\frac{\delta}{\delta A(t)}\int \mathrm{d}t \, \lambda(t)A^2(t). \tag{7.6}$$

Solving the derivative for the last term and inserting Eq. (7.4) results in

$$\frac{\delta}{\delta A(t)}\int \mathrm{d}\tau \, \mathrm{tr}\{\mathcal{O}(\tau)\rho_S(\tau)\} = \lambda(t)A(t). \tag{7.7}$$

Since the target operator is not affected by variations of the external field, the functional derivative applies only to the reduced density operator which is determined by Eq. (7.3). Thus, the derivative of the time-evolution superoperator (Fréchet derivative) can be straightforwardly computed as [MM01, MKM02]

$$\frac{\delta\rho_S(\tau)}{\delta A(t)} = \frac{\delta}{\delta A(t)}U(\tau, t_0, A)\rho(t_0)$$

$$
\begin{aligned}
&= -i\int_{t_0}^{\tau} \mathrm{d}t'\, U(\tau,t',A)\frac{\delta\mathcal{L}_\mu(t')}{\delta A(t)}U(t',t_0,A)\rho_S(t_0)\\
&= i\theta(\tau-t)U(\tau,t,A)\mathcal{L}_\mu U(t,t_0,A)\rho_S(t_0), \qquad (7.8)
\end{aligned}
$$

where $\theta(\tau-t)$ is the unit step function. Applying Eq. (7.8) to the kernel of Eq. (7.7) results in an explicit expression for the control field

$$
\begin{aligned}
A(t) &= \frac{i}{\lambda(t)}\int \mathrm{d}\tau\theta(\tau-t)\mathrm{tr}_S\{\mathcal{O}(\tau)U(\tau,t,A)\mathcal{L}_\mu U(t,t_0,A)\rho_S(t_0)\}\\
&= \frac{i}{\lambda(t)}\int \mathrm{d}\tau\theta(\tau-t)\mathrm{tr}_S\{\mathcal{O}(\tau)U(\tau,t,A)\mathcal{L}_\mu\rho_S(t)\}\\
&= \frac{i}{\lambda(t)}\int \mathrm{d}\tau\theta(\tau-t)\mathrm{tr}_S\{\overline{U}(\tau,t,A)\mathcal{O}(\tau)\mathcal{L}_\mu\rho_S(t)\}.
\end{aligned}
\qquad (7.9)
$$

The $\overline{U}(\tau,t,A)$ operator realizes a backward propagation from time t to the intermediate time τ and its existence can be proved by using the cyclic properties of the trace [MM01, MKM02]. It is not necessary to derive an explicit expression for $\overline{U}(\tau,t,A)$ since we only need an EOM for

$$
\chi(t) = \int \mathrm{d}\tau\,\theta(\tau-t)\overline{U}(\tau,t,A)\mathcal{O}(\tau), \qquad (7.10)
$$

which is derived in Appendix B.

Writing the result of Eq. (7.9) in terms of the auxiliary projector (7.10), the final expression for the optimal control field reads

$$
A(t) = \frac{i}{\lambda(t)}\mathrm{tr}_S\{\chi(t)\mathcal{L}_\mu\rho_S(t)\}. \qquad (7.11)
$$

Applying Eq. (7.11) to the master equation (7.1) results in an EOM for the reduced density operator

$$
\frac{\partial}{\partial t}\rho_S(t) = -i\mathcal{L}_{tb}\rho_S(t) - D(t)\rho_S(t) - \frac{1}{\lambda(t)}\mathrm{tr}_S\{\chi(t)\mathcal{L}_\mu\rho_S(t)\}\mathcal{L}_\mu\rho_S(t) \qquad (7.12)
$$

with an additional optimal control field term which includes the auxiliary operator $\chi(t)$ in its dipole part. The corresponding EOM for the auxiliary operator

$$
\frac{\partial}{\partial t}\chi(t) = -i\mathcal{L}_{tb}\chi(t) + \overline{D}(t)\chi(t) - \frac{1}{\lambda(t)}\mathrm{tr}_S\{\chi(t)\mathcal{L}_\mu\rho_S(t)\}\mathcal{L}_\mu\chi(t) + \mathcal{O}(t) \qquad (7.13)
$$

is determined by the total time-derivative of Eq. (7.10) and the dissipation operator $\overline{D}(t)$ is derived in more detail in Appendix B. The inhomogeneous term $\mathcal{O}(t)$ reflects the time-distributed target state within the system of EOM. Eq. (7.13) is propagated in the reverse time direction of Eq. (7.12) and since both equations depend on each other in their dipole field part, they cannot be propagated simultaneously. Thus, an iteration algorithm is required to solve this correlated system of equations.

7.2 Iteration algorithm

Similar to previous publications [MM01, MKM02, OZR99, SR90, XYO+04, Oht03, KM05b, KM05a], we solve the equation system for the optimal field applying an iteration algorithm which works as follows. We make an initial guess for the field $A^0(t) = \frac{i}{\lambda(t)}\mathrm{tr}_S\{\chi^0(t)\mathcal{L}_\mu\rho_S^1(t)\}$ to propage the EOM of the reduced density operator from t_0 to t_f utilizing

$$\frac{\partial}{\partial t}\rho_S^n(t) = -i\mathcal{L}_{tb}\rho_S^n(t) - D(t)\rho_S^n(t) - \frac{1}{\lambda(t)}\mathrm{tr}_S\{\chi^{n-1}(t)\mathcal{L}_\mu\rho_S^n(t)\}\mathcal{L}_\mu\rho_S^n(t), \qquad (7.14)$$

for $n = 1$. Here, n denotes the index of the iteration loop. $\rho_S^n(t)$ has to be saved at each time step in order to propagate the auxiliary operator (7.10) backwards from t_f to t_0 with

$$\frac{\partial}{\partial t}\chi^n(t) = -i\mathcal{L}_{tb}\chi^n(t) + \overline{D}(t)\chi^n(t) - \frac{1}{\lambda(t)}\mathrm{tr}_S\{\chi^n(t)\mathcal{L}_\mu\rho_S^n(t)\}\mathcal{L}_\mu\chi^n(t) + \mathcal{O}(t). \quad (7.15)$$

We also store the auxiliary operator for the next propagation of $\rho_S^n(t)$. In every iteration loop, we get two approximations for the control field, namely $A^n(t) = \frac{i}{\lambda(t)}\mathrm{tr}_S\{\chi^n(t)\mathcal{L}_\mu\rho_S^n(t)\}$ and $A^n(t) = \frac{i}{\lambda(t)}\mathrm{tr}_S\{\chi^{n-1}(t)\mathcal{L}_\mu\rho_S^n(t)\}$. Thus, back and forth iterations of expression (7.14) and (7.15) result in an iteration algorithm which maximizes the quantum mechanical observable of $\mathcal{O}(t)$. The initial value of the control field $A^0(t)$ can be set to zero or one can start with an approximate guess for an intuitive solution of the optimization problem.

7.3 Numerical results

In order to realize the optimal control algorithm described in the previous section, one simply has to add a routine which propagates Eq. (7.15) to the program code used for the calculations in chapter 6. A loop starts the two propagations one after another as it is described in section 7.2. The numerical difficulties are caused by the fact, that one has to define a discrete lattice in time to store the time-dependent dissipation operator $D(t)$ and the density operator $\rho(t)$. These values are needed for the next propagation of Eq. (7.15). The discrete time lattice requires a considerable amount of memory since one has to store a set of operators with dimension 2^N. On the other side, using a too wide lattice causes a numerical inhomogeneity which can even disturb the convergence behavior of the iteration algorithm. A partial solution to this problem would be to propagate the two dissipation operators $D(t)$ and $\overline{D}(t)$ independently in Eq. (7.14) and Eq. (7.15), leaving only the control field and the density operator to be saved. But this would slow down the algorithm by about a factor of two.

We employed the faster one of the two options and limit our calculations to small systems with either two or four sites. Also, influences caused by a phonon bath are neglected in this section. All calculations in this section are performed at a system temperature of $k_B T = 0.5\Delta$. As in chapter 6, we consider only one single Lorentzian for the spectral decomposition of the reservoirs and set the bandwidth to $\Gamma_1 = 40\Delta$. The weak coupling restriction was taken care of by applying Eq. (6.1). The employed dipole operator μ is given by Eq. (3.21).

Furthermore, the time-dependence of the target state $\mathcal{O}(t)$ is weighted with the Gaussian

$$F(t) = F_0 \exp\left(\frac{-(t - T_{peak})^2}{2\sigma_c^2}\right). \tag{7.16}$$

We will refer to $F(t)$ as target function. Thus, optimizations in regions of large $F(t)$ contribute more to the general control target $J_0(A)$ than contributions at small target function values. In this way, the algorithm can realize time-dependent control patterns determined by $F(t)$. In the following sections, neither F_0 nor $\int_\infty^\infty F(t)$ are normalized since the convergence behavior of the algorithm depends on the choice of F_0. Thus, $\mathcal{O}(t)$ and $J_0(A)$ are not normalized as well. But this does not affect the normalization of the other observables. Furthermore, a certain value for the initial control field is not chosen since the tested problems have simple geometries for which the algorithm showed a fast convergence. Thus, the initial control field was set to zero in the following numerical computations.

7.3.1 Optimal control of population without dissipation

The simplest nontrivial system within our framework is a wire consisting of two sites, which is not coupled to electron reservoirs or a phonon bath. The on-site energies are set equal $E_1 = E_2$. We employ this system to prove the convergence of the formalism and how well it realizes the time-dependent control target. In the initial state, the first site of the wire is occupied by a single electron, the second site is unoccupied. Then the system is propagated in time and the electron bounces between the two sites due to the hard wall boundary condition, as it is shown in the middle panel of Fig. 7.1. In order to access the population dynamics in the wire, the control target operator is set to

$$\mathcal{O}(t) = F(t) c_2^\dagger c_2. \tag{7.17}$$

The target function is given by Eq. (7.16) with the parameters $\sigma_c = 40$, $F_0 = 10$ and $T_{peak} = 300$, depicted in the upper panel of Fig. 7.1. Thus, the control target is to maximize the occupation level of site two at times when $F(t)$ has substantial values. The computed control field, depicted in the bottom panel of Fig. 7.1, applies

a sequence of short and irregular pulses to the wire which prohibit the electron from hopping back to site one. 800 iterations were executed for the computation.

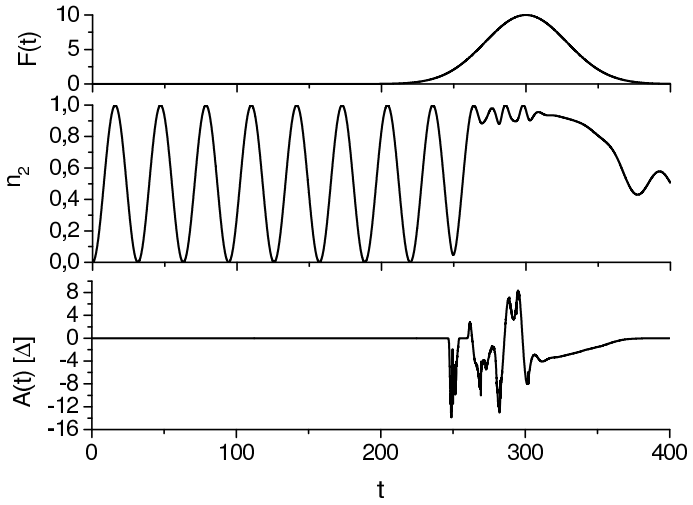

Figure 7.1: Optimal population control applied to a two site wire which is not coupled to electronic leads or a vibrational environment. The target function $F(t)$ is depicted in the upper panel. The population of site 2 in time is shown in the middle panel. Bottom panel: The state of the optimal control field after 800 iterations.

The mathematical origin of the control algorithm is the functional derivative of the objective control functional. This implies that the iteration algorithm has to increase monotonically the quantum mechanical expectation value defined by the control target [OZR99]. Fig. 7.2 shows an increase of the control parameter J_0 with each iteration step. The state depicted in Fig. 7.1 could be improved by further iterations since the maximal possible target value for the given system can be determined as

$$J_{0,max} = \int_{-\infty}^{\infty} \mathrm{d}t\, F(t) = 400\sqrt{2\pi} \approx 1000. \tag{7.18}$$

Here we used the fact, that the maximal occupation level at each site is limited to one. Especially additional pulses between $t = 200$ and $t = 250$ would improve the result since the occupation level in the tails of the Gaussian is relatively small. In general, we observed a faster convergence for narrower control functions. Thus, a smaller σ_c is applied in the following calculations.

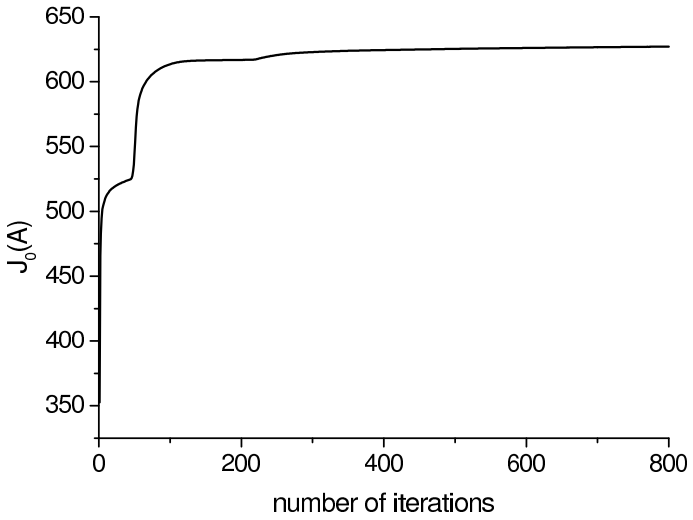

Figure 7.2: The monotonic convergence of the control algorithm given by Eqs. (7.14, 7.15). It was utilized to compute Fig. 7.1 which shows the state of the system after 300 iterations. The control target J_0 is defined by Eq. (7.5).

7.3.2 Optimal control of population with dissipation

Here, we employ the same system as in subsection 7.3.1 but with the sites coupled to two electron reservoirs as depicted in Fig. 3.1. The coupling is weaker than in the other calculations since we set $p_1 = 0.01\,(4\Delta\Omega_1\Gamma_1^2)$. The target function (7.16), shown in the upper panel of Fig. 7.3, is set up with the parameters $T_{peak} = 200$, $F_0 = 10$ and $\sigma_c = 10$ to enssure a fast convergence of the iteration algorithm. The control target operator is again given by Eq. (7.17). On the contrary to subsection 7.3.1, the initial reduced density matrix corresponds to the equilibrium state of the system which is determined by the influence of the two electronic leads, as it is described in section 6.1. Both leads are at the same Fermi energy $E_{F,l} = E_{F,r}$ and both sites have equal equilibrium occupation levels in the not irradiated wire. Thus, the solution to maximize the occupation level at the second site is to apply a constant laser pulse which lowers the on-site energy of this site. Since there is no dynamical bouncing of the population between the sites, a sequence of different pulses as in Fig. 7.1 is not required.

The maximal control target is given by $J_{0,max} = 100\sqrt{2\pi} \approx 251$. Fig. 7.4 depicts the convergence of the iteration algorithm applied to compute the state shown in Fig. 7.3. The algorithm finds the obvious solution to the problem immediately and

one observes a fast convergence at the beginning. It slows down later when only minor adjustments to the control field are made by the algorithm.

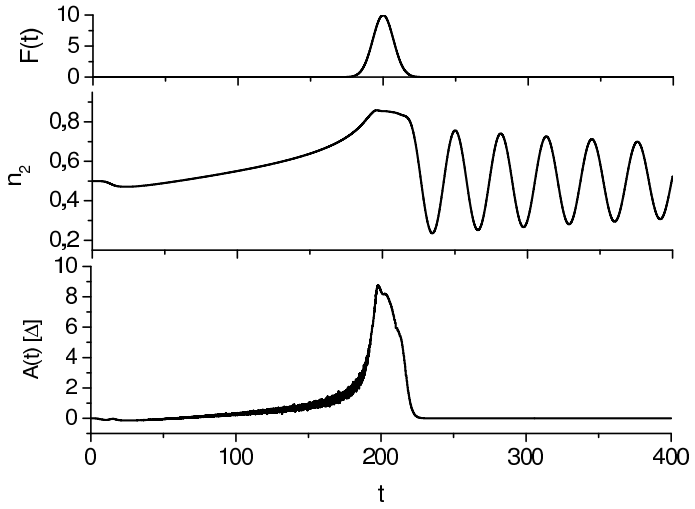

Figure 7.3: Similar situation as in Fig. 7.1, but with two leads attached to the wire. The equilibrium state of the system without external field was employed as the initial state of the wire. 200 iterations were performed to compute the control field shown in the bottom panel.

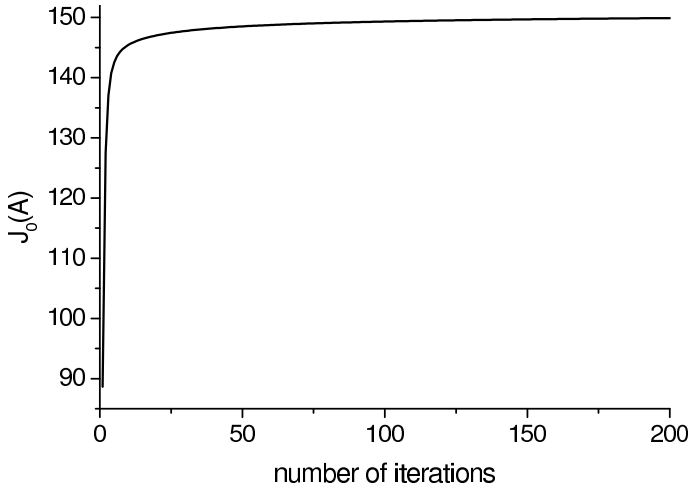

Figure 7.4: The convergence of the control algorithm used to optimize the population dynamics of a wire coupled to two electron reservoirs, depicted in Fig. 7.3.

7.3.3 Optimal control of current

7.3.3.1 Current switching

In order to realize a control scheme for the net current through a molecular wire, one just has to apply the net current operator $\mathcal{I}_{net}(t) = \frac{1}{2}(\mathcal{I}_l(t) + \mathcal{I}_r(t))$ for the control target operator

$$\mathcal{O}(t) = F(t)\mathcal{I}_{net}(t). \tag{7.19}$$

The parameters of the target function $F(t)$, displayed in the upper panel of Fig. 7.5, are given by $\sigma_c = 5.0$, $F_0 = 10$ and $T_{peak} = 200$. The major difference to the control of population dynamics is that the current operator is time-dependent as well. It is propagated simultaneously with Eq. (7.14), stored and then applied during the propagation of Eq. (7.15).

The on-site energies of the wire are configured as in Fig. 6.6 with $U_{12} = E_1 - E_2 = -4\Delta$ and a bias voltage of $E_{F,l} - E_{F,r} = 2\Delta$ is additionally applied to the system. The equilibrium net current which corresponds to this energy configuration can be computed as $I_{equilibrium} \approx 1.910^{-4}\,[\mathrm{I}]$. An intuitive solution for a high equilibrium conductance of the wire would be to apply a constant amplitude of $A = 4\Delta$ to the dipole operator (3.21), which would align the on-site energies $E_1 = E_2$. In this case, the numerically computed net current is given by $I_{equilibrium} \approx 5.1910^{-3}\,[\mathrm{I}]$. Since the initial density matrix does not match with the equilibrium density matrix of the system, one can observe current fluctuation in the third panel of Fig. 7.5 between $t = 0$ and $t = 25$.

We use this configuration in order to check whether the formalism finds the solution by itself for this simple problem. The bottom panel of Fig. 7.5 displays the computed control field amplitude $A(t)$ after 100 iterations. The solution of the algorithm is even better than the intuitive one, viz. aligning the on-site energies, and it can be understood by looking at the population dynamics shown in the second panel of Fig. 7.5. First, the left wire site is charged until it almost reaches its maximal occupation level. Then the short pulse depicted in the bottom panel of Fig. 7.5 with a peak amplitude of about $A_{peak} = 6\Delta$ discharges site one and pumps the population to site two. This realizes the short current peak depicted in the third panel of Fig. 7.5. The algorithm also accounts for the inertia of the system by applying the pulse before the control target function $F(t)$ has significant values. Thus, we see the current peak at exactly $T_{peak} = 200$. The width of the current distribution shows also a good agreement with the desired shape.

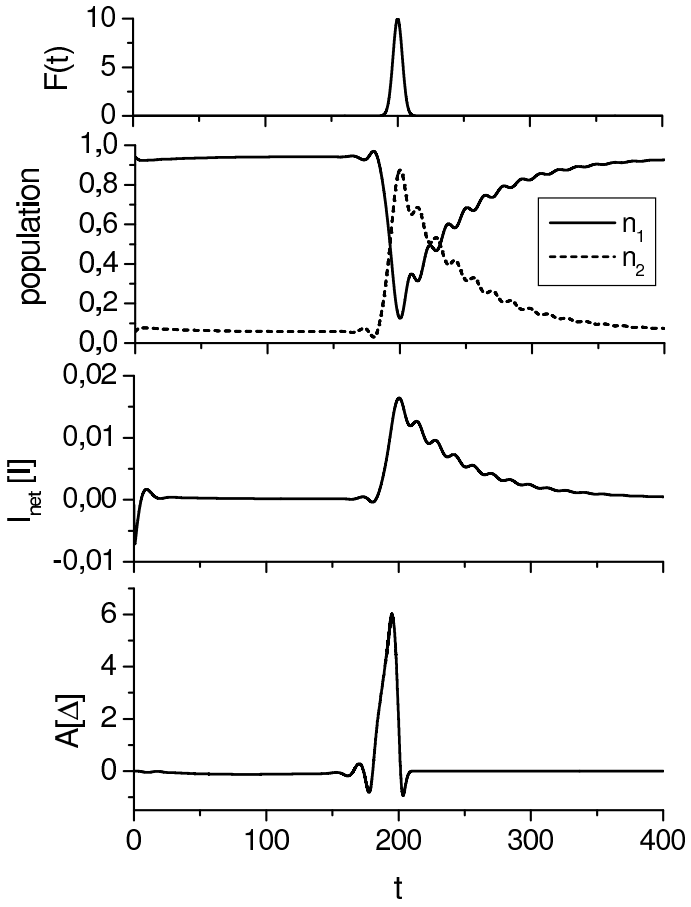

Figure 7.5: The laser assisted transport through a wire with asymmetric on-site energies $U_{12} = E_1 - E_2 = -4\Delta$. A bias voltage of $E_{F,l} - E_{F,r} = 2\Delta$ is applied to the wire. The upper panel depicts the control target function $F(t)$, the population of the two sites and the net current are shown in the second and third panel, respectively. 100 iterations were executed to compute the control field shown in the bottom panel.

The convergence behavior of the algorithm employing the current operator, depicted in Fig. 7.6, is quite similar to calculations employing a non-timedependent particle number operator (7.17), where one could achieve a fast convergence by defining a narrow and simple control function pattern. It is monotonic increasing which shows the numerical stability of the algorithm also for time-dependent target operators, if the time lattice in which the operators are stored is smooth enough.

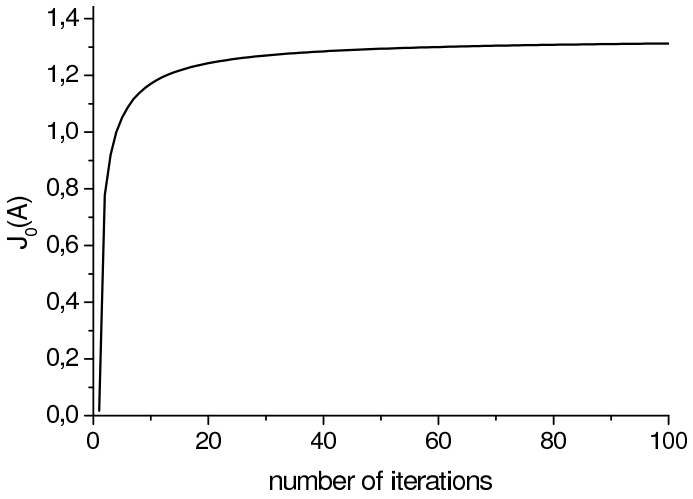

Figure 7.6: The convergence of the optimal control algorithm which was used to compute the control field shown in Fig. 7.5.

7.3.3.2 Laser driven current

In the previous subsection, a situation was given where a bias voltage caused current whose value was then influenced by an optimally controlled external laser field. Here we want to present a study where the current is driven by the laser field only without the support of a bias voltage. Therefore the left and the right Fermi energies are set equal and a tight binding Hamiltonian consisting of four sites at equal on-site energies is employed. The outermost sites have fixed energies while the inner sites are subject to the dipole operator

$$\mu = \frac{e}{2}\left(x_2 + x_3\right) \tag{7.20}$$

which is modulated with the amplitude of the laser field as it is described in Eq. (3.19). The scaled positions x_n are given by Eq. (3.22). The target of the optimal control algorithm is to achieve a current surge determined by the target function $F(t)$ depicted in the upper panel of Fig. 7.7. Its parameters are given by $\sigma_c = 5.0$, $F_0 = 0.5$ and $T_{peak} = 200$.

The problem is different from the previous examples since an optimized current spike at $T_{peak} = 200$, as shown in the third panel of Fig. 7.7, cannot be achieved by applying only a single pulse as in the previous subsection. Hence a more complicated solution for the control field is derived by the control algorithm, depicted in the bottom panel of Fig. 7.7. It can be understood by considering the population dynamics of the wire, depicted in the second panel of Fig. 7.7. The reason for the

first pulses is to induce bouncing electron waves in the wire between the left and right lead. Since the wire-lead coupling is weak, a portion of a wave of population travelling through the wire cannot enter the lead and therefore bounces back. The waves which are propagating through the wire are increased with every pulse in order to have a favorable distribution of momenta and position in the wire before the current spike at $t = 200$ is due. Then, similar to the previous cases, a major field pulse causes a major current spike. The propagating waves engender a series of current surges in regular patterns before and after the main current peak.

After the field is turned off, the electron waves start decaying while causing an alternating current. Fig. 7.7 was taken after 50 iterations and the peak of the current surge does match the maximum of the control function $F(t)$. A good timing of the field is required in this model since the height and shape of the final current spike also strongly depend on the sequence of the previous pulses. There is also a longer delay between the main field pulse and the measured current since the electrons have to pass an additional site before they are measured by entering or leaving the electron reservoirs. The convergence of the OCT algorithm is shown in Fig. 7.8. The prospective of electrical current driven by an optimal external field in a molecular junction promises a variety of applications since the energy of the EM field is directly transformed into an electrical current without the need of an initial bias voltage or certain molecular symmetry.

In conclusion, we have derived an optimal control algorithm for the electrical current in molecular systems and demonstrated its applicability for simple and comprehensible systems. This should enable future investigations to deal with more complicated and realistic systems, which would also engender more complex control fields. Another aspect is to include also the phonon bath into the optimal control calculations. A time-reverse dissipation operator for the phonon bath coupling can be derived in the same way as $\overline{D}(t)$ for the electron reservoirs. A study of the vibrational coupling promises a variety of effects within the optimal control theory but a full discussion would exceed the frame of this work.

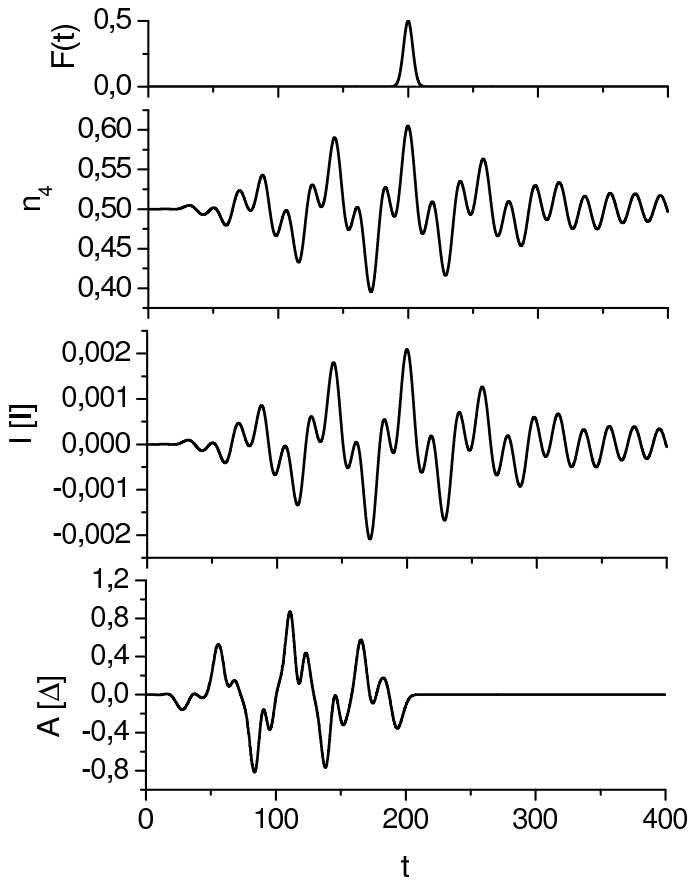

Figure 7.7: Optimal control of a 4-site wire where the laser field depicted in the bottom panel influences only site 2 and 3. The on-site energies are equal and no bias voltage is applied $E_1 = E_2 = E_3 = E_4 = E_{F,l} = E_{F,r}$. The upper panel depicts the control target function $F(t)$, the population of site 4 and the net current are shown in the second and third panel, respectively. 50 iterations were executed to compute the control field.

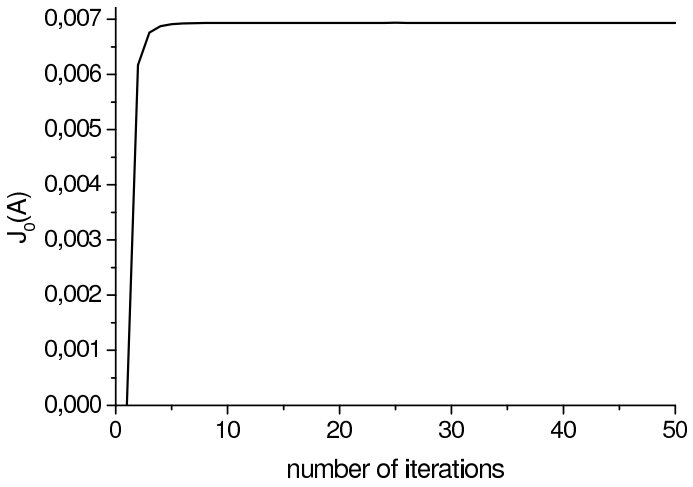

Figure 7.8: The convergence of the optimal control algorithm which was used to compute Fig. 7.7.

Chapter 8

SUMMARY AND PERSPECTIVE

We have developed a time-dependent non-Markovian conduction formalism based on a projection operator approach for the density matrix with a numerical decomposition of the spectral density. It enables studies of the time-resolved current and population dynamics in molecular wires for arbitrary time-dependent wire Hamiltonians, a powerful extension to existing theories and applicable for a wide range of systems. The formalism includes the coupling to the electronic leads and to the phonon bath in second-order perturbation theory and a non-perturbative interaction with external fields. The resulting transport formalism could become a powerful tool in mesoscopic physics if certain extensions are made. Its validity was demonstrated numerically for different examples like the coherent destruction of tunneling in a driven two-state system, optical control of current using a short laser pulse, alternating currents and the electrical relaxation of the system into a biased equilibrium state.

These effects were investigated on a femtosecond time scale, which is an important aspect for its applicability to cover fast dynamical aspects. We furthermore made a comparison of TNL and TL approaches to conclude that both agree in the case of weak wire reservoir coupling. With the improved optimal control formalism, we were able to determine optimized control fields realizing a well defined time-distributed target state such as a short current peak. Thus, we introduced an often applied method in chemistry and molecular dynamics to the field of molecular electronics.

The scientific achievements of this thesis

- Development of a method mathematically similar to the approach of Meier and Tannor to account for the electron transfer in time-dependent open quantum systems.

- Employment of their method to include vibrational coupling in a molecular wire.
- Derivation of a current equation in consistence with our theory for the electron transfer.
- Obtainment of a current operator by changing to a TL approach.
- Determination of an optimal control formalism for the open system electron transfer in order to deal with time-dependent target states.
- Extension of our model to deal with time-dependent electron reservoirs.
- Realization of the points listed above numerically and presentation of basic transport problems.
- Presentation of results for the influence of short laser pulses on the electrical current in molecular wires.

Future investigations should extend the method to more sophisticated control goals which would allow the formalism to deal with highly complicated current patterns. Also, most of the examples presented refer only to simple physical situations since we used them primarily to show the applicability of the method. Improved calculations should include more realistic spectral densities, i.e. an Ohmic spectral density for the vibrational coupling and a wire-lead transmission spectrum taken from experimental data for the spectral density of the leads.

The role of the vibrational coupling in the electron transfer should be addressed in more detail since it is not completely clear how the phonon bath influences the electrical current in dynamical situations. The prospective of including an additional electron-electron interaction would further complement the quantum mechanical description of the system.

Starting from the definition of the current operator, one can develop a theory to calculate the current fluctuation occurring during the transport. This noise information and the extracted Fano factor would yield a deeper physical understanding of effects like CDT [CKH04]. A formal improvement of the derived method would be to prove that it can be embedded in other quantum transport theories, e.g. Landauer-Büttiker, similar to Refs. [LLY$^+$05, CLSY].

From a numerical point of view, a major issue for optimization is to deal with the Matsubara frequencies and the FFR values in a different way as it is done in the

presented work. For wide bands and low temperatures, the requirement of a large number of Matsubara/FFR terms slows down the code significantly. One possible solution to reduce their number could be a partial integration of the auxiliary density matrices.

Many system properties in mesoscopic physics require a higher system dimensionality. Since a two-dimensional tight-binding description in matrix form requires an extensive mapping between the sites, a Fock space basis is not applicable anymore. Although it would be accompanied by a loss of generality, another modification would be to replace the Fock space by a different basis which scales for instance with N^2 or N instead of 2^N in the 1D case.

Appendix A

THE UNIT SYSTEM AND PARAMETERS

In this section, we shortly present a way how to derive the macroscopic equivalents of the units which we used in the current formalism by setting $\hbar = k_B = 1$. The numerical results are all expressed in terms of the hopping parameter Δ acting as the free parameter to gauge the system. Taking $\Delta = 0.1$ eV is as reasonable value for molecular systems, a temperature of

$$k_B T = 0.25\Delta$$

then corresponds to

$$T = 290.2\,\mathrm{K}.$$

If we set the driving frequency of the external field to

$$E = \hbar\omega_d = 10\Delta,$$

the corresponding wave length λ is determined through the dispersion relation of light

$$\lambda \frac{\Omega}{2\pi} = c$$

what results in

$$\lambda = \frac{2\pi c\hbar}{10 \cdot 0.1\,\mathrm{eV}} = 1243\,\mathrm{nm}.$$

Furthermore, the period time for a single oscillation is given by

$$T_{period} = \frac{\lambda}{c} = 4.14\,\mathrm{fs}$$

for infrared light with a wave length of $\lambda = 1243\,\mathrm{nm}$. Now, we can use this light beam to measure the time unit for the employed time parameter t. In the program code used for the numerical calculations, ω_d is set to

$$\omega_d = 1.0.$$

Thus, the time unit of the program simply becomes

$$[t] = \frac{T_{period}}{2\pi} = 0.659\,\text{fs}.$$

After determining the time, the current unit of the system $[I]$ can be derived from the basic definition of the current, namely

$$[I] = \frac{Q}{t} = \frac{e}{t} = \frac{1.6 \cdot 10^{-19}\,\text{C}}{0.659\,\text{fs}} = 2.43 \cdot 10^{-4}\,\text{A}.$$

Other values like the parameters for the spectral decomposition, the on-site energy or Fermi energy are of the order of eV in the system of interest and are therefore expressed directly in terms of Δ.

Appendix B

TIME REVERSE AUXILIARY OPERATOR

The calculations executed in Eq. (7.9) utilized the existence of a time reverse time-propagation operator $\overline{U}(\tau, t, A)$. In this section, we employ the abbreviation $B(t) = \mathcal{L}_\mu(t)\rho_S(t)$. In order to derive a differential expression for (7.10), one has to refer to the time derivative applied to the time-propagation operator in the trace expression of Eq. (7.9). Thus, we get

$$\begin{aligned}
\tfrac{\partial}{\partial t}\mathrm{tr}_S\left\{\mathcal{O}(\tau)U(\tau,t,A)B(t)\right\} &= \mathrm{tr}_S\left\{\mathcal{O}(\tau)U(\tau,t,A)(i\mathcal{L}_{tb}+i\mathcal{L}_\mu(t)+D(t))B(t)\right\} \\
&= \mathrm{tr}_S\left\{U^\dagger(\tau,t,A)\mathcal{O}(\tau)\left(i\mathcal{L}_{tb}+i\mathcal{L}_\mu(t)+D(t)\right)B(t)\right\} \\
&= \mathrm{tr}_S\left\{\chi(t)\left(i\mathcal{L}_{tb}+i\mathcal{L}_\mu(t)+D(t)\right)B(t)\right\}. \qquad \text{(B.1)}
\end{aligned}$$

The trace can be separated into the wire part and the dissipation part and both can be evaluated separately. The Liouville operator can be shifted into the first position in the trace utilizing the transformations

$$\begin{aligned}
i\mathrm{tr}_S\left\{\chi(t)\mathcal{L}(t)B(t)\right\} &= i\mathrm{tr}_S\left\{\chi(t)(H(t)B(t)-B(t)H(t))\right\} \\
&= i\mathrm{tr}_S\left\{\chi(t)H(t)B(t)-H(t)\chi(t)B(t)\right\} \\
&= i\mathrm{tr}_S\left\{-\mathcal{L}(t)\chi(t)B(t)\right\}. \qquad \text{(B.2)}
\end{aligned}$$

The time-reverse dissipation operator is given by

$$\begin{aligned}
&\mathrm{tr}_S\left\{\chi(t)D(t)B\right\} \\
=\ &\sum_{xx'}\mathrm{tr}_S\left\{\chi(t)(K_x\Lambda_{xx'}(t)B-K_xB\widehat{\Lambda}_{xx'}(t)-\Lambda_{xx'}(t)BK_x+B\widehat{\Lambda}_{xx'}(t)K_x\right\} \\
=\ &\sum_{xx'}\mathrm{tr}_S\left\{\chi(t)K_x\Lambda_{xx'}(t)B-\widehat{\Lambda}_{xx'}(t)\chi(t)K_xB-K_x\chi(t)\Lambda_{xx'}(t)B+\widehat{\Lambda}_{xx'}(t)K_x\chi(t)B\right\} \\
=\ &\sum_{xx'}\mathrm{tr}_S\left\{\overline{D}(t)\chi(t)B\right\}. \qquad \text{(B.3)}
\end{aligned}$$

with

$$\overline{D}(t)\chi(t)=\sum_{xx'}\widehat{\Lambda}_{xx'}(t)K_x\chi(t)-K_x\chi(t)\Lambda_{xx'}(t)-\widehat{\Lambda}_{xx'}(t)\chi(t)K_x+\chi(t)K_x\Lambda_{xx'}(t). \qquad \text{(B.4)}$$

These are the necessary terms for the EOM (7.13) of the $\chi(t)$ operator.

SELBSTSTÄNDIGKEITSERKLÄRUNG

Hiermit erkläre ich, dass ich die vorliegende Arbeit selbstständig angefertigt, nicht anderweitig zu Prüfungszwecken vorgelegt und keine anderen als die angegebenen Hilfsmittel verwendet habe. Sämtliche wissentlich verwendete Textausschnitte, Zitate oder Inhalte anderer Verfasser wurden ausdrücklich als solche gekennzeichnet.

Sven Welack

ACKNOWLEDGMENT

I want to thank Professor Michael Schreiber for giving me the opportunity to write my diploma thesis in his group and for his enduring support during my time in Chemnitz. Thanks for the permanent efforts to create an excellent scientific environment in Chemnitz.

Further I want to thank my thesis supervisor Dr. Ulrich Kleinekathöfer for many inspiring discussions, his commitment to my project and thoughtful research ideas which are the foundations of this work. Thanks also for the organization of the very exciting workshop in Dresden which showed me the greater scheme of my work and introduced me to the scientific community.

Thanks to Markus Schröder for his infinite amount of patience helping me to become comfortable with the theoretical foundations of dissipative quantum mechanics.

Thanks also to Dr. Sigmund Kohler, Dr. Klaus Morawetz and Dr. Reinhardt Scholz for many useful discussions.

I would like to thank my office colleagues for the great moments and discussions we had together, viz. Afshin Abbasi, Alexey Novikov, Alexander Terentyev, Bernd Schmidt, Carsten Olbrich, Davoud Pouladsaz, Guang Qi Li, Luis Mancera, Linus Gisslen, Peter Karmann, Soroosh Pezeshki and Victor Cerovski as well as Alexander Croy and Christoph Sormann in Warwick.

Special thanks to Phillip Cain, whose competence with computers provided the excellent facilities which made the numerical part of this thesis possible.

I am also very grateful to Prof. Branislav Nikolić at University of Delaware for his support during my time in Delaware and afterwards. Thanks for the personal and scientific guidance which he provides to his group as an outstanding mentor and researcher. He introduced me to the world of research and also showed me the beauty of quantum mechanics, which gave me with the right spirit for this thesis.

Also best wishes for the future to my friends and office colleagues at UD Adebanjo Oriade, Adrian Gorea, Eugeniya Tchoukova, Liviu Zârbo, Rupsi Chandra, Ralitsa

Dragomirova, Thomas Ekiert and everybody I forgot to mention, and thank you for the great time and the international experience.

Thanks also to the Studienstiftung des deutschen Volkes for accepting me as a fellow and for introducing me to this group of bright and open minded students.

Finally, I want to thank my family consisting of my father Henry, my mother Marion, my brother Jens, my sister Tina, my grandparents Emil, Ursula and Elfriede and my uncle Uwe, aunt Ute and cousin Anja for their unselfish support over the last decades.

PUBLICATIONS OF THE AUTHOR

1 Sven Welack, Michael Schreiber, and Ulrich Kleinekathöfer: *The influence of ultra-fast laser pulses on electron transfer in molecular wires studied by a non-Markovian density matrix approach*, cond-mat/0509442

2 Sven Welack, Ulrich Kleinekathöfer, and Michael Schreiber: *Laser-driven molecular wires studied by a non-Markovian density matrix approach*, Journal of Luminescence (accepted)

3 Branislav Nikolić, Liviu Zârbo, and Sven Welack: *Transverse Spin-Orbit Force in the Spin Hall Effect in Ballistic Semiconductor Wires*, Phys. Rev. B. **72**, 075335 (2005).

PRESENTATIONS AND TALKS OF THE AUTHOR RELATED TO THIS WORK

1 Talk, Group seminar *"Order, Disorder and Chaos"* of the Theory of Disordered Systems Group (THUS) at TU-Chemnitz, June 2005

2 Poster presentation, International workshop *"Classical and Quantum Dynamical Simulations in Chemical and Biological Physics* at the MPI-PKS Dresden, June 2005

3 Poster presentation, Annual spring meeting of the German Physical Society (DPG) in Berlin, March 2005

LIST OF FIGURES

BIBLIOGRAPHY

[AR74] A. Aviram and M.A. Ratner: *Molecular Rectifiers*, Chem. Phys. Lett., 29: 277, 1974.

[Bal98] L. E. Ballentine: *Quantum Mechanics - A Modern Development*, World Scientific Publishing, Singapore, 1998.

[BBS97] P. Brune, C. Bruder and H. Schoeller: *Photo-assisted transport through ultrasmall quantum dots: Influence of intradot transitions*, Phys. Rev. B, 56: 4730, 1997.

[BILP85] M. Buettiker, Y. Imry, R. Landauer and S. Pinhas: *Generalized many-channel conductance formula with application to small rings*, Phys. Rev. B, 31: 6207, 1985.

[BKP99] H. P. Breuer, B. Kappler and F. Petruccione: *Stochastic wave-function method for non-Markovian quantum master equations*, Phys. Rev. A, 59: 1633, 1999.

[Blu96] K. Blum: *Density Matrix Theory and Applications*, Plenum Press, New York, 2nd Edition, 1996.

[BS89] H. U. Baranger and A. D. Stone: *Electrical linear-response theory in an arbitrary magnetic field: A new Fermi-surface formation*, Phys. Rev. B, 40: 8169, 1989.

[BS93] C. Bruder and H. Schoeller: *Charging Effects in Ultrasmall Quantum Dots in the Presence of Time-Varying Fields*, Phys. Rev. Lett., 72: 1076, 1993.

[Bue86] M. Buettiker: *Four-Terminal Phase-Coherent Conductance*, Phys. Rev. Lett., 57: 1761, 1986.

[Čáp94] V. Čápek: *Interplay of exciton or electron transfer and relaxation I. Mori approach*, Physica A, 203: 520, 1994.

[CDM97] R. I. Cukier, C. Denk and M. Morillo: *Control of tunneling processes with an external field in a four-level system: an analytic approach*, Chem. Phys., 217: 179, 1997.

[CKH04] S. Camalet, S. Kohler and P. Hänggi: *Shot-noise control in ac-driven nanoscale conductors*, Phys. Rev. B, 70: 155326, 2004.

[CLKH03] S. Camalet, J. Lehmann, S. Kohler and P. Hänggi: *Current Noise in ac-Driven Nanoscale Conductors*, Phys. Rev. Lett., 90: 210602, 2003.

[CLSY] P. Cui, X. Q. Li, J. Shao and Y.J. Yan: *Quantum Transport from the Perspective of Quantum Open Systems*, cond-mat/0506477.

[CPZ+01] X.D. Cui, A. Primak, X. Zarate, J. Tomfohr, O.F. Sankey, A.L. Moore, D. Gust, G. Harris and S.M. Lindsay: *Reproducible Measurement of Single-Molecule Conductivity*, science, 294: 571, 2001.

[DA92] S. Datta and M.P. Anantram: *Steady-state transport in mesoscopic systems illuminated by alternating fields*, Phys. Rev. B, 45: 13761, 1992.

[Dak94] J. Dakhnovskii: *Nonadiabatic chemical reactions in a strong time-dependent electric field: An electron transfer reaction in a polar solvent*, J. Chem. Phys., 100: 6492, 1994.

[Dat95] S. Datta: *Electronic transport in mesoscopic systems*, Cambridge University Press, Cambridge, 1995.

[DGO+95] M. Dorogi, J. Gomez, R. Osifchin, R.P. Andres and R. Reifenberger: *Room-temperature Coulomb blockade from a self-assembled molecular nanostructure*, Phys. Rev. B, 52: 9071, 1995.

[EPR35] A. Einstein, B. Podolsky, and N. Rosen: *Can Quantum-Mechanical Description of Physical Reality Be Considered Complete?*, Phys. Rev., 47: 777, 1935.

[EWK04] F. Evers, F. Weigend and M. Koentopp: *The conductance of molecular wires and DFT based transport calculations*, Phys. Rev. B, 69: 235411, 2004.

[GDDN04] A. W. Ghosh, P. S. Damle, S. Datta and A. Nitzan: *Molecular Electronics: Theory and Device Prospect*, MRS Bulletin, 6: 391, 2004.

[GDJH91] F. Grossmann, T. Dittrich, P. Jung and P. Hänggi: *Coherent Destruction of Tunneling*, Phys. Rev. Lett., 67: 516, 1991.

[GGS02] F. Grossmann, R. Gutiérrez and R. Schmidt: *Conductance Calculations for Real Systems on the Nanoscale*, ChemPhysChem, 3: 650, 2002.

[GH98] M. Grifoni and P. Hänggi: *Driven Quantum Tunneling*, Phys. Rep., 304: 229, 1998.

[GKS95] E. Geva, R. Kosloff and J. L. Skinner: *On the relaxation of a two-level system driven by a strong electromagnetic field*, J. Chem. Phys., 102: 8541, 1995.

[GN] M. Galperin and A. Nitzan: *Current induced light emission and light induced current in molecular tunneling junctions*, cond-mat/0503114v2.

[GPM96] I. A. Goychuk, E. G. Petrov and V. May: *Control of the dynamics of a dissipative two-level system by a strong periodic field*, Chem. Phys. Lett., 253: 428, 1996.

[Haa73] F. Haake: Springer Tracts Mod. Phys., 66: 98, 1973.

[Hof63] R. Hoffman: *An Extended Hückel Theory. I. Hydrocarbons*, J. Chem. Phys., 39: 1397, 1963.

[Iij91] S. Iijima: *Helical microtubules of graphitic carbon*, Nature, 354: 56, 1991.

[IL99] Y. Imry and R. Landauer: *Conductance viewed as transmission*, Rev. Mod. Phys., 71: 306, 1999.

[INT] *For further details, http://www.intel.com/technology/silicon/micron.htm and http://www.intel.com/technology/magazine/silicon/moores-law-0405.htm.*

[JDHD98] J. Jersch, F. Demming, L.J. Hildenhagen and K. Dickmann: *Field enhancement of optical radiation in the nearfield of scanning probe microscope tips*, Appl. Phys. A, 66: 29, 1998.

[JGSC95] C. Joachim, J. K. Gimzcwski, R. R. Schlittler and C. Chavy: *Electronic Transparance of a Single C_{60} Molecule*, Phys. Rev. Lett., 74: 2102, 1995.

[JR92] R.S. Judson and H. Rabitz: *Teaching lasers to control molecules*, Phys. Rev. Lett., 68: 1500, 1992.

[KARM02] A. Keller, O. Atabek, M. Ratner and V. Mujica: *Laser assisted conductance of molecular wires*, J. Phys. B: Mol. Opt. Phys., 35: 4981, 2002.

[KBH+03] U. Kleinekathöfer, I. Barvík, P. Herman, I. Kondov and M. Schreiber: *Memory Effects in the Fluorescence Depolarization Dynamics Studied within the B850 Ring of Purple Bacteria*, J. Phys. Chem., 107: 14094, 2003.

[KBP+99] C. Kergueris, J.-P. Bourgoin, S. Palacin, D. Esteve, C. Urbina, M. Magoga and C. Joachim: *Electron transport through a metal-molecule-meta junction*, Phys. Rev. B, 59: 12505, 1999.

[KCS+04] S. Kohler, S. Camalet, M. Strass, J. Lehmann, G.L. Ingold and P. Hänggi: *Charge transport through a molecule driven by a high-frequency field*, Chem. Phys., 296: 243, 2004.

[KFZ+00] J. Kong, N. R. Franklin, C. Zhou, M. G. Chapline, S. Peng, K. Cho and H. Dai: *Nanotube Molecular Wires as Chemical Sensors*, Science, 287: 622, 2000.

[Kle04] U. Kleinekathöfer: *Non-Markovian theories based on the decomposition of the spectral density*, J. Chem. Phys., 121: 2505, 2004.

[KLH05] S. Kohler, J. Lehmann, and P. Hänggi: *Driven quantum transport on the nanoscale*, Phys. Rep., 406: 379, 2005.

[KM05a] A. Kaiser and V. May: *Optimal control theory for a target state distributed in time: Optimizing the probe-pulse signal os a pump-probe-scheme*, J. Chem. Phys., 121: 2528, 2005.

[KM05b] A. Kaiser and V. May: *Optimizing frequency dispersed transient absorption signals: A computational study*, Chem. Phys. Lett., 405: 339, 2005.

[KSA+] S. Kurth, G. Stefanucci, C.-O. Almbladh, A. Rubio and E. K. U. Gross: *Time-dependent quantum transport: A practical scheme using density functional theory*, cond-mat/0502391.

[Lan57] R. Landauer: *Spatial Variation of Currents and Fields Due to Localized Scatterers in Metallic Conduction*, IBM J. Res. Develop., 1: 233, 1957.

[LCKH03] J. Lehmann, S. Camalet, S. Kohler and P. Hänggi: *Laser controlled molecular switches and transistors*, Chem. Phys. Lett., 368: 282, 2003.

[LIH02] J. Lehmann, G.-L. Ingold and P. Hänggi: *Incoherent charge transport through molecular wires: interplay of Coulomb interaction and wire population*, Chem. Phys., 281: 199, 2002.

[LKHN02] J. Lehmann, S. Kohler, P. Hänggi and A. Nitzan: *Molecular wires acting as coherent quantum ratchets*, Phys. Rev. Lett., 88: 228305, 2002.

[LKHN03] J. Lehmann, S. Kohler, P. Hänggi and A. Nitzan: *Rectification of laser-induced electronic transport through molecules*, J. Chem. Phys., 118: 3283, 2003.

[LKMH04] J. Lehmann, S. Kohler, V. May and P. Hänggi: *Vibrational effects in laser-driven molecular wires*, J. Chem. Phys., 121: 2278, 2004.

[LLY+05] X.-Q. Li, J.-Y. Luo, Y.-G. Yang, P. Cui and Y. Yan: *Quantum master equation approach to quantum transport through mesoscopic systems*, Phys. Rev. B, 71: 205304, 2005.

[MK00] V. May and O. Kühn: *Charge and Energy Transfer in Molecular Systems*, Wiley-VCH, Berlin, 2000.

[MKM02] T. Mančal, U. Kleinekathöfer and V. May: *Femtosecond Laser Pulse Control of Electron Transfer*, J. Chem. Phys., 117: 636, 2002.

[MKR94] V. Mujica, M. Kemp and M. A. Ratner: *Electron conduction in molecular wires. I. A scattering formalism*, J. Chem. Phys., 101: 6849, 1994.

[MM01] T. Mančal and V. May: *Laser Pulse Control of Ultrafast Electron Transfer Reactions*, Eur. Phys. J. D, 14: 173, 2001.

[Moo65] G. E. Moore: *Cramming more components onto integrated circuits*, Electronics, 38: 114, 1965.

[MOR78] S. Mukamel, I. Oppenheim and J. Ross: *Statistical reduction for strongly driven simple quantum systems*, Phys. Rev. A, 17: 1988, 1978.

[MT99] C. Meier and D. J. Tannor: *Non-Markovian evolution of the density operator in the presence of strong laser fields*, J. Chem. Phys., 111: 3365, 1999.

[Nak58] S. Nakajima: *On quantum theory of transport phenomena*, Prog. Theor. Phys., 20: 948, 1958.

[Nit01] A. Nitzan: *Electron transmission through molecules and molecular interfaces*, Ann. Rev. Phys. Chem., 52: 681, 2001.

[NR03] A. Nitzan and M. A. Ratner: *Electron Transport in Molecular Wire Junctions*, Science, 300: 1384, 2003.

[Oht03] Y. Ohtsuki: *Non-Markovian effects on quantum optimal control of dissipative wave packet dynamics*, J. Chem. Phys., 119: 661, 2003.

[ON05] I. V. Ovchinnikov and D. Neuhauser: *Finite bias conductance of an Anderson level: A source-Liouville Hartree Fock study*, J. Chem. Phys., 122: 024707, 2005.

[OZR99] Y. Ohtsuki, W. Zhu and H. Rabitz: *Monotonically convergent algorithm for quantum optimal control with dissipation*, J. Chem. Phys., 110: 9825, 1999.

[RBN97] D. R. Reichman, F. L. H. Brown and P. Neu: *Cumulant expansions and the spin-boson problem*, Phys. Rev. E, 55: 2328, 1997.

[ROW+02] J. Reichert, R. Ochs, H. B. Weber, M. Mayor and H. von Löhneysen: *Driving Current through Single Organic Molecules*, Phys. Rev. Lett., 88: 176804, 2002.

[RSK+] M. Rey, M. Strass, S. Kohler, F. Sols and P. Hänggi: *Transport suppression in heterostructures driven by an ac gate voltage*, cond-mat/0412221.

[RZM+97] M. A. Reed, C. Zhou, C. J. Muller, T. P. Burgin and J. M. Tour: *Conductance of a Molecular Junction*, Science, 278: 252, 1997.

[SM98] D. Schirrmeister and V. May: *Femtosecond pulse dependence of dissipation in molecular systems*, Chem. Phys. Lett., 297: 383, 1998.

[SNU+02] R. H. M. Smit, Y. Noat, C. Untiedt, N. D. Lang, M. C. Hemert and J. M. van Ruitenbeek: *Measurement of the conductance of a hydrogen molecule*, Nature, 419: 906, 2002.

[SR90] S. Shi and H. Rabitz: *Quantum mechanical optimal control of physical observables in microsystems*, J. Chem. Phys., 92: 364, 1990.

[SVR99] K. Sundermann and R. Vivie-Riedle: *Extension to quantum optimal control algorithms and applications to special problems in state selective molecular dynamics*, J. Chem. Phys., 110: 1896, 1999.

[TDD+97] S. J. Tans, M. H. Devoret, H. Dai, A. Thess, R. E. Smalley, L. J. Geerligs and C. Dekker: *Individual single-wall carbon nanotubes as quantum wires*, Nature, 386: 477, 1997.

[TDH+98] W. Tian, S. Datta, S. Hong, R. Reifenberger, J.I. Henderson and C.P. Kubiak: *Conductance spectra of molecular wires*, J. Chem. Phys., 109: 7, 1998.

[TKR86] D. J. Tannor, R. Kosloff and S. A. Rice: *Coherent pulse sequence induced control of selectivity of reactions: Exact quantum mechanical calculations*, J. Chem. Phys., 85: 5805, 1986.

[UV02] C.A. Ullrich and G. Vignale: *Time-dependent current-density-functional theory for the linear response of weakly disordered systems*, Phys. Rev. Lett., 65: 245102, 2002.

[WAB+01] S. A. Wolf, D. D. Awschalom, R. A. Buhrman, J. M. Daughton, S. von Molnár, M. L. Roukes, A. Y. Chtchelkanova and D. M. Treger: *Spintronics: A Spin-Based Electronics Vision for the Future*, Science, 294: 1488, 2001.

[WJM93] N.S. Wingreen, A. Jauho and Y. Meir: *Time-dependent transport through a mesoscopic syste*, Phys. Rev. B, 48: 8487, 1993.

[WWR05] E.A. Weiss, M.R. Wasielewski and M.A. Ratner: *"Molecular wires: Molecule-Assisted Movement of Charge and Energy"*, Top Curr Chem, 257: 103, 2005.

[XY02] R. Xu and Y. J. Yan: *"Theory of open quantum systems"*, J. Chem. Phys., 116: 9196, 2002.

[XYO+04] R. Xu, Y. J. Yan, Y. Ohtsuki, Y. Fujimura and H. Rabitz: *Optimal control of quantum non-Markovian dissipation: Reduced Liouville-space theory*, J. Chem. Phys., 120: 6600, 2004.

[Yan93] Y. J. Yan: *Optimal control of molecular dynamics via two-photon processes*, J. Chem. Phys., 100: 1094, 1993.

[Yan98] Y. J. Yan: *"Quantum Fokker-Planck theory in a non-Gaussian-Markovian medium"*, Phys. Rev. A, 58: 2721, 1998.

[YPF+03] H. Yan, S. H. Park, G. Finkelstein, J. H. Reif and T. H. LaBean: *DNA-Templated Self-Assembly of Protein Arrays and Highly Conductive Nanowires*, Science, 301: 1882, 2003.

[YX05] Y. J. Yan and R.X. Xu: *Quantum Mechanics of Dissipative Systems*, Ann. Rev. Phys. Chem., 56: 187, 2005.

[ŽFS04] I. Žutić, J. Fabian and S. D. Sarma: *Spintronics: Fundamentals and applications*, Rev. Mod. Phys., 76: 323, 2004.

[Zwa61] R. Zwanzig: in *Lectures in Theoretical Physics* (edited by W. E. Brittin, B. W. Downs and J. Downs), 3, 106, Interscience, New York, 1961.

[Zwa64] R. Zwanzig: *On the identity of three generalized master equations*, Physica, 30: 1109, 1964.